

1 Late Pleistocene glacial chronologies and paleoclimate in the
2 northern Rocky Mountains

3 **Brendon J. Quirk^{1,2*}**, Elizabeth ~~Huss~~²~~Huss~~³, Benjamin J.C. Laabs³, Eric Leonard⁴, Joseph
4 **Licciardi⁵**, Mitchell A. Plummer⁶, Marc W. ~~Caffee~~⁷~~Caffee~~^{8,2}

5 ¹ *Department of Geology and Geophysics, University of Utah, Salt Lake City, Utah 84112, USA*

6 ²~~Department~~² *Department of Earth, Atmospheric, and Planetary Sciences, Purdue University,*
7 *West Lafayette, Indiana 47905, USA*

8 ³~~Department~~ *of Geosciences, State University of New York at Geneseo, Geneseo, NY 14454, USA*

9 ³~~Department~~⁴~~Department~~ *of Geosciences, North Dakota State University, Fargo, North Dakota*
10 *58102, USA*

11 ⁴~~Department~~⁵~~Department~~ *of Geology, Colorado College, Colorado Springs, Colorado 80903,*
12 *USA*

13 ⁵~~Department~~⁶~~Department~~ *of Earth Sciences, University of New Hampshire, Durham, New*
14 *Hampshire 03824, USA*

15 ⁶~~Idaho~~⁷~~Idaho~~ *National Engineering and Environmental Laboratory, Idaho Falls, Idaho 83415,*
16 *USA*

17 ⁷~~Department~~⁸~~Department~~ *of Physics and Astronomy, PRIME Lab, Purdue University, West*
18 *Lafayette, Indiana 47905, USA*

19

20 **Corresponding author email address: bjquirk@purdue.edu*

Formatted: Superscript

21 **ABSTRACT**

22 The geologic record of mountain glaciations is a robust indicator of terrestrial paleoclimate
23 change. During the last glaciation, mountain ranges across the western U.S. hosted glaciers while
24 the Cordilleran and Laurentide ice sheets flowed to the west and east of the continental divide,
25 respectively. Records detailing the chronologies and paleoclimate significance of these ice
26 advances have been developed for many sites across North America. However, relatively few
27 glacial records have been developed for mountain glaciers in the northern Rocky Mountains near
28 ~~former~~ ice sheet margins. Here, we report cosmogenic beryllium-10 surface exposure ages and
29 numerical glacier modeling results ~~showing~~ which show that mountain glaciers in the northern
30 Rockies abandoned terminal moraines after the end of the global Last Glacial Maximum around
31 17-18 ka and could have been sustained by -10 to -8.5°C temperature depressions relative to
32 modern assuming similar or ~~drier~~ less than modern precipitation. Additionally, we present a
33 deglacial chronology from the northern Rocky Mountains that indicates while there is
34 considerable variability in initial moraine abandonment ages across the Rocky Mountains, the
35 pace of subsequent ice retreat through the Lateglacial exhibits some regional coherence. Our
36 results provide insight on potential regional mechanisms driving the initiation of and sustained
37 deglaciation in the western U.S. including rising atmospheric CO₂ and ice sheet collapse.

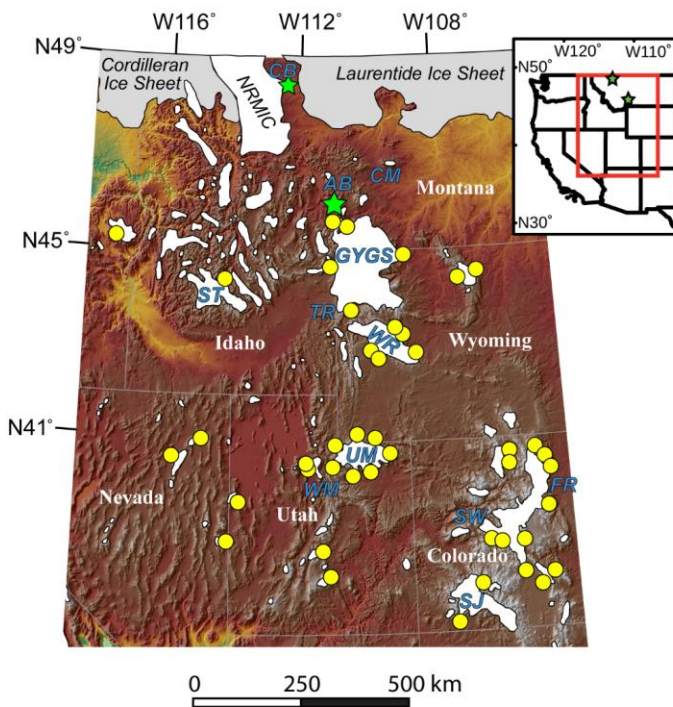
38 **INTRODUCTION**

39 Mountain glaciers are widely recognized as robust indicators of modern climate change
40 (Oerlemans, 2005; Vaughan et al., 2013; Mark and Fernández, 2017). Investigations of past glacier
41 fluctuations preserved in the geologic record can ~~therefore~~ reveal valuable information regarding
42 past climate oscillations and variability (e.g. Gilbert, 1890; Blackwelder, 1931; McCoy et al.,
43 1985; Marcott et al., 2019). In the Rocky Mountain region of the western U.S., records of

44 mountain glaciation have been used extensively to reconstruct the regional pattern of Pleistocene
45 glaciation in space and time (e.g., Porter et al., 1983; Leonard, 1989; Licciardi et al., 2004; Laabs
46 et al., 2009; Quirk et al., 2020), but few studies have focused on northern ranges along the former
47 southern margins of the Laurentide and Cordilleran ice sheets. While surficial geologic records of
48 Pleistocene mountain glaciation in the northern Rocky Mountains of western Montana have been
49 available for decades (Alden, 1932; Carrara, 1987), these records have seldom been used to infer
50 Pleistocene-climate conditions (e.g., Murray and Locke, 1989). Many ranges were occupied by
51 coalesced valley glaciers and ice caps with high-altitude ice divides, which are especially difficult
52 to reconstruct based solely on mapped glacial deposits and landforms. Additionally, in much of
53 northwestern Montana, mountain glaciers likely coalesced with the southern edges of the
54 Laurentide and Cordilleran ice sheets, which also complicates reconstructions of paleo-glaciers,
55 and limits the usefulness of traditional methods for inferring past climate from glacier equilibrium-
56 line altitudes or mass-balance gradients.

57 However, discrete Pleistocene mountain glaciers occupied some ranges of western
58 Montana, as evidenced by a well-preserved record of deposits and landforms delimiting their
59 maximum extent during the last glaciation. Such records are found in the northern Absaroka Range
60 in southwestern Montana and the eastern Lewis Range in northwestern Montana (Figure 1), where
61 glaciers incised deep valleys and in some areas constructed broad terminal moraine complexes
62 along mountain fronts. These records present an opportunity to reconstruct mountain glacier
63 extents and develop cosmogenic chronologies of the last glaciation. These spatiotemporally
64 constrained paleo-glaciers can then, in turn, be used to infer paleoclimate conditions in the northern
65 Rocky Mountains during the last glaciation—for which relatively few records exist compared to
66 other regions of western North America.

67 Here we present new surficial mapping of latero-terminal moraines of the last Pleistocene
68 glaciation in the Cut Bank and Lake Creek valleys in the eastern Lewis Range and cosmogenic
69 ¹⁰Be surface exposure ages of a terminal moraine complex in Cut Bank valley. For the northern
70 Absaroka Range, we present new exposure ages for latero-terminal moraines in South Fork Deep
71 Creek and Cascade Creek valleys as well as glacially scoured bedrock ages from Pine Creek to
72 track ice retreat from a previously dated terminal moraine to a cirque floor. We use the
73 spatiotemporal glacial histories from the Lewis and Absaroka ranges to inform numerical
74 modeling of paleo-glacier shapes, thicknesses and paleoclimate conditions (i.e., precipitation and
75 temperature) for mapped and dated glacial stadials. We then compare the glacial chronologies and
76 glacier-climate modeling results developed for the Lewis and northern Absaroka Ranges to those
77 from other western North America mountain ranges and examine how these glacial histories can
78 inform our understanding of regional patterns of glaciation and climate change.



79
 80 *Figure 1. Pleistocene ice extents in the northern U.S. Rocky Mountains (after Pierce et al., 1983;*
 81 *Pierce, 2003) with the locations of our two field sites, Cut Bank Creek (CB) in the Lewis Range*
 82 *and Pine Creek, South Fork Deep Creek, and Cascade Creek in the northern Absaroka Range*
 83 *(AB) indicated by green stars. Locations of previously established age control are indicated by*
 84 *yellow circles including the Greater Yellowstone glacial system (GYGS), Crazy Mountains (CM),*
 85 *Wind River (WR), Sawtooth (ST), Wasatch (WM), Uinta (UM), Front Range (FR), Sawatch (SW),*
 86 *and San Juan (SJ) ranges. General outlines of the Cordilleran and Laurentide ice sheets as well*
 87 *the northern Rocky Mountain ice cap (NRMIC) are also shown. (Inset) Map of Western North*
 88 *America with state outlines. Green stars indicate our study areas and the red box shows the*
 89 *approximate coverage of the main illustration.*

90

91 **Site ~~Description~~ Descriptions**

92 The Lewis Range ([48.5°N, 113.5°W](#)) hosted numerous glaciers [during the latest](#)
93 [Pleistocene](#) and, in some areas, [these glaciers](#) coalesced ~~forming to form~~ the northern Rocky
94 Mountain ice cap ([Locke, 1995](#); Figure 1). In this study, we focus on the Cut Bank Creek glacier
95 which flowed east from its headwaters at 2.6 km asl and terminated on the piedmont just above
96 1.4 km asl at its maximum extent. The Cut Bank glacier did not coalesce with either the northern
97 Rocky Mountain ice cap to the west and north or the Laurentide ice sheet to the east during
98 Pinedale times and flowed as a discrete mountain glacier- ([Calhoun, 1906](#); [Alden, 1932](#)). The
99 glacier was ~~over 25~~ [nearly 30](#) km long at its maximum extent and in many areas was over 200
100 meters thick with maximum ice thickness in excess of 300 meters [as evidenced from apparent](#)
101 [trimline elevations and other glacial features identified in the valley \(Carrara, 1989\). Modern](#)
102 [average temperatures near Cut Bank Creek range from approximately -5°C in December to 15°C](#)
103 [in July \(NOAA COOP #242626, East Glacier, 1466 m asl\). Annual precipitation on average is](#)
104 [around 715 mm with more than 60% occurring between October and March.](#)

105 The Absaroka Range, ([45°N, 110.6°W](#)), located to the north of the Greater Yellowstone
106 glacial system (Figure 1) also hosted several glaciers during Pinedale times including the Pine
107 Creek, South Fork Deep Creek, and Cascade Creek glaciers. The three glaciers flowed from
108 southeast to the northwest just to the range front where they built terminal and lateral moraine
109 complexes- ([Weed, 1893](#); [Pierce, 1973](#); [Pierce, 1979](#) and references therein). All three canyons
110 have headwaters at or above 3 km asl and generally flowed down to elevations of around 1.6-1.7
111 km asl. The Pine Creek Pinedale glacier was the longest of the three at over 13 km at ~~its~~
112 maximum extent. The Cascade and South Fork Deep Creek glaciers were around 6 and 7 km

113 long at their maximum Pinedale extents, respectively. Ice thicknesses were thinner in the
114 Absaroka Range glaciers ~~as~~ compared to the Cut Bank glacier, with many areas hosting 100-200
115 meter thick ice and maximum thicknesses in Pine Creek of 250-300 meters-[\(Licciardi et al.,
116 2001; Licciardi and Pierce 2008\). Modern average temperatures near the Absaroka Range range
117 from approximately -3°C in December to 19°C in July \(NOAA COOP #245080, Livingston,
118 1484 m asl\). On average, annual precipitation is around 412 mm.](#)

119 **Previous Studies**

120 Reconstructions of Pleistocene glaciers in the northern Rocky Mountains of western
121 Montana are limited (Pierce, 2003), and relatively little work has been done inferring past climate
122 in the region from paleoglacier characteristics. Most previous work has focused either on the
123 Greater Yellowstone area of southern Montana or on the Glacier National Park area of northern
124 Montana – also the foci of the current study. In these and other areas of western Montana past
125 workers have identified deposits and landforms from the penultimate and most recent glaciations,
126 generally termed Bull Lake and Pinedale glaciations, following the terminology developed by
127 Blackwelder (1915) for the Wind River Range of Wyoming (Fig. 1). Based on chronologies of
128 glacial deposits throughout the Middle and Southern Rocky Mountains, these last two Pleistocene
129 glaciations are thought to correspond broadly with intervals of global ice volume increase during
130 marine isotope stages (MIS) 2 and 6, respectively (Licciardi and Pierce, 2008; Licciardi and Pierce,
131 2018; Quirk et al., 2018; Dahms et al. 2018; Schweinsberg et al., 2020; Laabs et al., 2020).
132 Chronological work utilizing cosmogenic nuclide surface-exposure dating in the
133 Yellowstone/Grand Teton National Parks area of southwestern Montana and adjacent
134 northwestern Wyoming (Licciardi et al., 2001; Licciardi and Pierce, 2008, 2018; Pierce et al.,
135 2018) has allowed subdivision of Pinedale-age deposits as is discussed below.

136 Deposits of Pleistocene mountain glaciers in the eastern Lewis Range of western Montana
137 were mapped and described as early as 1906 by Calhoun and then later by Alden (1932), Carrara
138 (1989), and Fullerton et al. (2004). Calhoun (1906) described the broad hummocky terminal and
139 recessional moraines deposited on the plains to the east of Cut Bank Creek headwaters investigated
140 in this study as well as several recessional moraine ridges deposited up valley. Fullerton et al.
141 (2004) ~~identified~~inferred multiple Pinedale tills, two ages of Bull Lake till, and a possible pre-Bull
142 Lake till in moraine deposits at Cut Bank Creek and elsewhere along the eastern front of the Lewis
143 Range. No numerical ages are available for these deposits, although a radiocarbon age on a wood
144 fragment, underlying two latest Pleistocene tephra layers in lake sediment at Marias Pass, provides
145 a minimum age of $12,194 \pm 145$ ^{14}C yr (Carrara, 1995) or ~~~13.8-14.245.8 cal yr/kyr~~ (Fullerton et al.,
146 2004; recalibrated here using IntCal13 (1 σ); Reimer et al., 2013) for complete recession of at least
147 one east-side outlet glacier of the Northern Montana Ice Cap in the Glacier National Park region.

148 Pleistocene glacial deposits north of Yellowstone National Park and near the northern
149 Absaroka Range were first described and mapped by Weed (1893) and then later by Pierce (1973;
150 1979 and references therein). Licciardi and Pierce (2018) identified three distinct phases of
151 glaciation in the Greater Yellowstone region during the last glacial including the early (22-18 ka),
152 middle (18-16 ka), and late (16-13 ka) Pinedale. While the early Pinedale phase in the Yellowstone
153 area occurred mainly during the ~~interval of the global~~ Last Glacial Maximum, defined as the period
154 of greatest global ice-volume during the most recent glacial stage (26.5-19.0 ka; Clark et al., 2009);
155 the middle and late Pinedale phases clearly postdated the global LGM, although they appear to
156 have predated the Younger Dryas interval. Terminal and recessional moraines at the southwestern
157 front of the northern Absaroka Range and in ~~the neighboring~~ Paradise Valley to the south ~~of~~have
158 cosmogenic ^{10}Be exposure ages that were originally reported by Licciardi et al. (2001) and

159 ~~combined~~ have been supplemented with additional data ~~by~~ from Licciardi and Pierce (2008; 2018).
160 The terminal moraine in Pine Creek valley of the northern Absaroka Range has a mean cosmogenic
161 ¹⁰Be exposure age of 18.2 ± 0.5 ka (± 1 standard error of the mean) ~~as~~ recalculated using methods
162 described in the ~~text~~ Methods section. In Paradise Valley, moraines delimiting the terminus of the
163 northern outlet of the Yellowstone glacial system have mean ¹⁰Be exposure ages of 17.9 ± 0.4 ka
164 for the Eightmile terminal moraine and 17.1 ± 0.6 ka for the Chico recessional moraine. ~~Together,~~
165 ~~these~~ Here, we interpret exposure ages ~~indicate that mountain glaciers in this sector of a~~ ice retreat
166 or moraine abandonment ages. Thus, the exposure ages from the Greater Yellowstone glacial
167 system suggest that mountain glaciers began retreating from their terminal moraines during the
168 middle Pinedale and ~~critically,~~ after the end of the global Last Glacial Maximum.

Formatted: Superscript

169 While many investigations in western Montana have focused on reconstructing the extent
170 and chronology of the Pinedale glaciation, fewer have attempted to describe Pinedale climate
171 conditions. Less attention has been paid by previous workers to use of paleoglaciological methods
172 to reconstruct late Pleistocene climate in western Montana than to reconstruction of the extent and
173 chronology of past glaciation. Locke (1990) examined modern and reconstructed late Pleistocene
174 glacier equilibrium lines throughout western Montana, concluding that an assumed late Pleistocene
175 temperature depression of 10°C would have been associated with decreased precipitation relative
176 to the present. Based on mapping of glacial deposits and landforms in the Crazy Mountains of
177 southwestern Montana (Figure 1), Murray and Locke (1989) reconstructed the geometry and ice
178 flux of a valley glacier in Big Timber Canyon. They ~~interpret~~ interpreted the reconstructed ice-
179 surface gradient and ice flux as indicators of a cold and dry regional climate during the last
180 glaciation. Hostetler & Clark (1997) used a combination of climate-model output and glacier
181 equilibrium-line modeling and concluded that during the LGM in the Yellowstone region summer

182 temperatures were 10-15°C colder than present with winter precipitation approximately equal to
183 present, while in northern Montana winter temperature depression was even greater but
184 precipitation was reduced compared to modern.

185 ~~Nowhere in the U.S. northern Rocky Mountains have more recent~~
186 ~~paleoglaciological~~Modern methods, ~~used to reconstruct paleo-glaciers,~~ particularly distributed
187 energy/mass-balance ~~models~~ or degree-day mass-balance models, ~~been applied to reconstructed~~
188 ~~late Pleistocene glaciers, as they~~ have been successfully applied ~~to sites~~ in the Middle ~~Rocky~~
189 ~~Mountains~~ (Laabs et al., 2006; Refsnider et al., 2008; Birkel et al., 2012; Quirk et al., 2018, 2020)
190 and Southern Rocky Mountains (Ward et al., 2009; Brugger, 2010; Brugger et al. 2018, 2019;
191 Dühnforth and Anderson, 2011; Leonard et al., 2014, 2017a; Schweinsberg et al., 2016; ~~et al.~~). In this
192 study we apply a modified version of the Plummer and Phillips (2003) distributed energy/mass-
193 balance model to reconstructed glaciers in the Absaroka and Lewis ranges to help elucidate climate
194 conditions in the northern Rockies during the last glaciation.

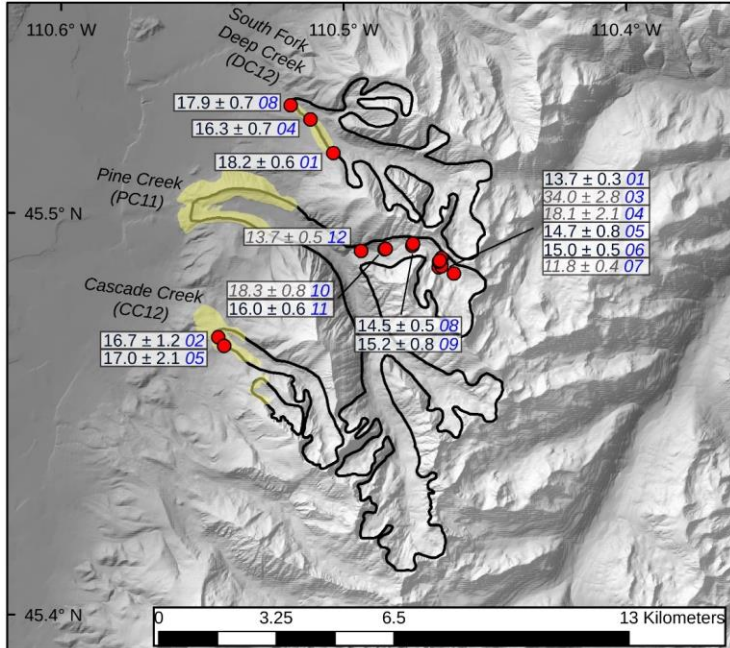
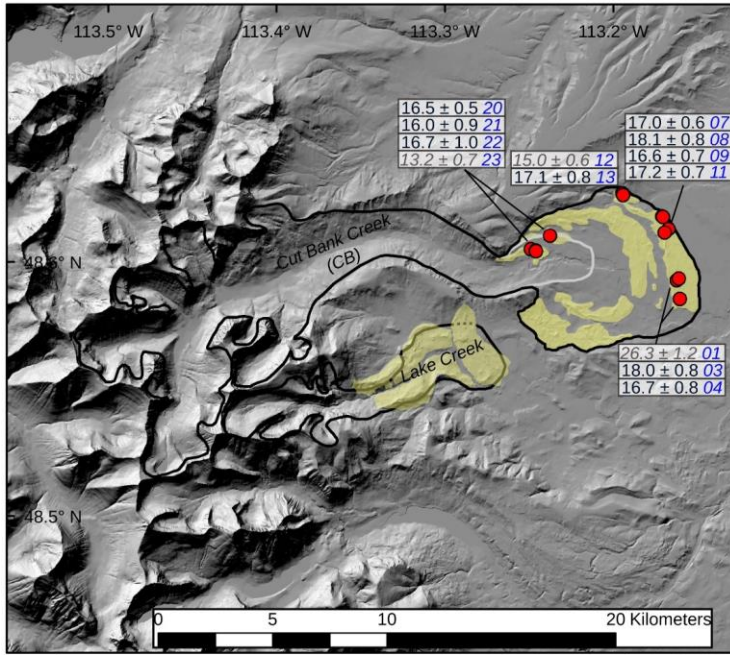
195 .

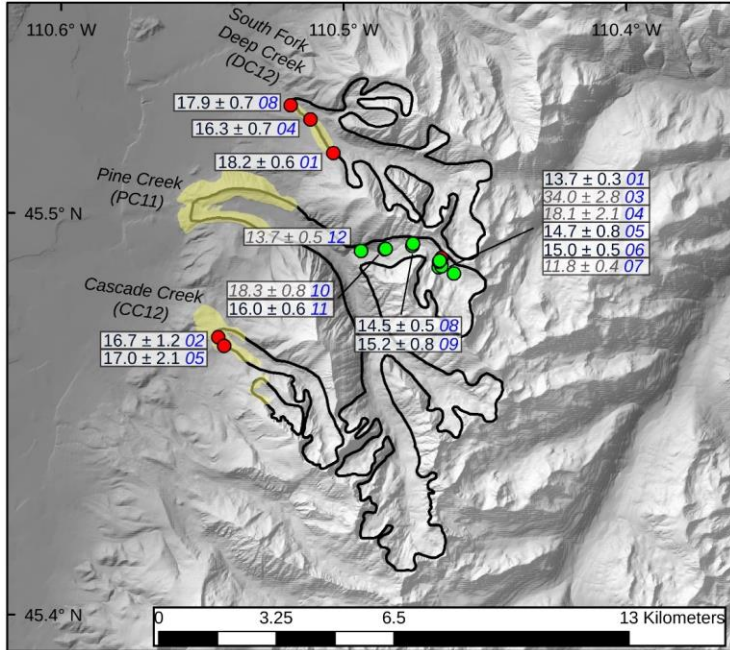
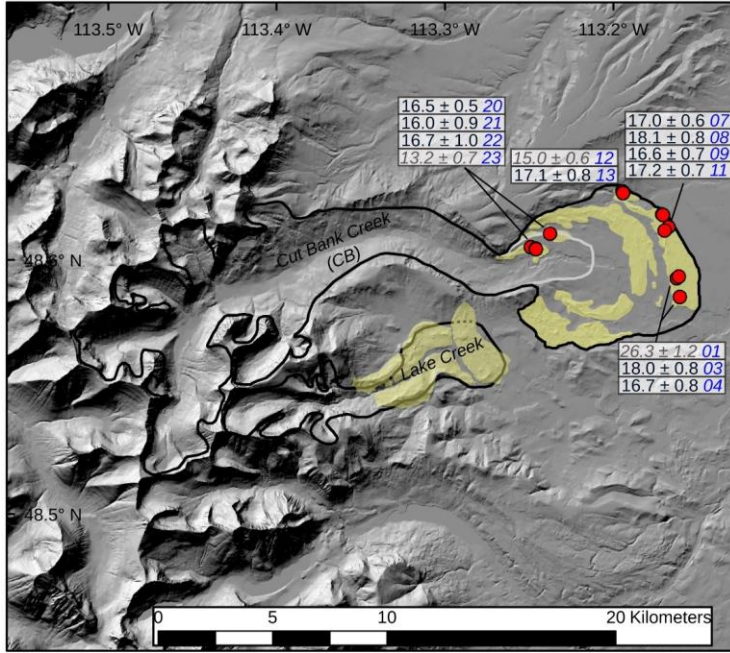
196 **METHODS**

197 **Moraine Mapping**

198 Although terminal moraines of east-flowing glaciers in the Lewis Range are known from
199 previous studies, they were remapped here to aid with reconstructing maximum ice extent in the
200 Cut Bank Creek and Lake Creek valleys (Figure 2a). Moraines in both valleys were examined in
201 aerial imagery available in Google Earth and using 1:24,000-scale topographic maps. The portion
202 of the terminal moraine north of Cut Bank Creek was mapped in the field. Moraines were identified
203 as broad (0.5-1 km wide), looping plateaus with hummocky topography (Figure 3) on the piedmont
204 east of the Lewis Range and featured abundant erratic boulders ~~at~~on their crests.

205 Surficial mapping of glacial deposits within our area of interest in the Absaroka Range had
206 been previously completed by Pierce (1979 and references therein). Mapping in the Pine Creek
207 area was subsequently updated by Licciardi and Pierce (2008). In the field, we checked and
208 confirmed, without modification, the moraine mapping from these previous studies.





211 *Figure 2. (Top) Cut Bank Creek study area located in the Lewis Range of northern Montana.*
212 *(Bottom) northern Absaroka Range study area including South Fork Deep Creek, Pine Creek, and*
213 *Cascade Creek drainages. Pinedale maximum ice extents are outlined in black (dashed where*
214 *inferred). Recessional position at Cut Bank outlined in light-grey. Moraine deposits are shown in*
215 *yellow ~~with~~ cosmogenic ¹⁰Be boulder and bedrock sample locations are indicated by ~~the~~ red and
216 green circles, respectively, with exposure ages (Promontory Point calibration data and LSD
217 scaling scheme) and analytical uncertainty (shown in ka) and sample codes in blue text. Exposure
218 *ages interpreted as outliers are shown in grey and italicized.**



219
 220 *Figure 3. (A) Characteristic hummocky morphology of Cut Bank Creek terminal moraine. (B)*
 221 *Boulder CB-03 targeted for cosmogenic exposure dating on the Cut Bank terminal moraine. (C)*
 222 *Photograph taken facing north-northeast looking across the threshold of Pine Creek Lake and*
 223 *towards bedrock sampled for cosmogenic exposure dating. (D) Location of bedrock sample PC11-*

224 11. (E) Lateral sector of the Cascade Canyon Pinedale terminal moraine. (F) South Fork Deep
225 Creek lateral moraine sample DC12-01.

226 **Cosmogenic ¹⁰Be Exposure Dating**

227 Following moraine mapping and field verification, we selected moraines and erratic
228 boulders atop moraine crests for *in-situ* cosmogenic ¹⁰Be exposure dating to determine landform
229 ages- at Cut Bank Creek, South Fork Deep Creek, and Cascade Creek canyons. We targeted two
230 frontal moraines at Cut Bank Creek including the ice-distal terminal moraine. Boulders atop a
231 recessional moraine identified just beyond the mouth of Cut Bank Canyon were also sampled to
232 limit the time when moraine building at the mountain front ceased and ice retreat commenced. At
233 South Fork Deep Creek and Cascade Creek, we targeted lateral moraines associated with
234 maximum mapped ice extents. We collected samples from bedrock and erratic boulders not
235 associated with moraine deposits along a transect of Pine Creek canyon.

236 On moraine crests, we searched for large (>0.5 m tall), quartz-bearing boulders with broad
237 horizontal surfaces. When possible, we selected boulders and bedrock surfaces with clear glacial
238 polish and/or striations. In the northern Absaroka Range, most sampled moraine-boulders
239 consisted of Jewel Quartzite (Archean rocks of the Wyoming Province; Zientek et al., 2005), which
240 generally contains >90% quartz and some accessory minerals. In the Cut Bank Creek valley,
241 sampled moraine boulders consisted of silica-cemented quartz arenite derived from the Appekunny
242 Formation (subdivided from the Proterozoic Belt Supergroup), which is widely exposed along
243 bedrock divides in the Lewis Range (Whipple et al., 1984). By selecting only samples with clear
244 glacial polish and/or striations we determined that sample surface erosion was insignificant, and
245 we therefore used an erosion rate of 0 cm a⁻¹ in exposure age calculations. Samples were collected
246 using a hammer and chisel to depths ranging from 1 – 5 cm, with an average depth of 3 cm. The

247 number of samples collected from each landform varied based on the availability of suitable
248 targets. Topographic shielding data were collected in the field with a clinometer. Target surfaces
249 were selected so as to minimize the effect of internal shielding and cosmic ray scattering from
250 nearby boulders.

251 At Pine Creek in the northern Absaroka Range, where cosmogenic ^{10}Be exposure ages of
252 latero-terminal moraines were already available (Licciardi and Pierce, 2008), glacially scoured
253 bedrock and erratic boulders were sampled along the path of ice retreat. Here, we assume that
254 bedrock surfaces became progressively exposed through time as ice retreated up valley from the
255 terminal moraine and, therefore, exposure ages would limit the pace and timing of ice retreat (cf.
256 Guido et al., 2007). Jewel Quartzite, described above, bedrock and erratic boulders were sampled
257 along the length of the transect and were collected following the same procedure described above.

258 All samples were prepared at SUNY Geneseo for in-situ cosmogenic ^{10}Be measurement
259 following methods in Laabs et al. (2013). Samples were crushed, milled, and sieved to a target
260 grain size of 250-500 μm . Quartz grains were isolated using a rare earth hand magnet, Franz
261 magnetic separator, density separation, and dilute acid treatment. The quartz purification process
262 was accomplished by repeated etching in dilute hydrofluoric and nitric acids (Kohl and Nishiizumi,
263 1992). Prior to dissolution in concentrated hydrofluoric acid, the purified quartz fraction of each
264 sample was spiked with a commercially made ^9Be carrier solution purchased from SPEX CertiPrep
265 with a certified Be concentration of 1 mg/mL. Procedural blanks were prepared using equal carrier
266 mass as was added to samples. The beryllium fraction of each sample was chemically isolated and
267 loaded into targets for $^{10}\text{Be}/^9\text{Be}$ measurement by accelerator mass spectrometry (AMS) at the
268 Purdue University Rare Isotope Measurement Laboratory (Sharma et al., 2000; Muzikar et al.,

269 2003). All $^{10}\text{Be}/^9\text{Be}$ values were normalized to the AMS beryllium standard 07KNSTD
270 (Nishiizumi et al., 2007).

271 We calculated cosmogenic ^{10}Be exposure ages using the Balco et al. (2008) online
272 exposure age calculator, version 3.0 (<http://hess.ess.washington.edu/math/>). This calculator and
273 version were selected because they implement the Lifton-Sato-Dunai nuclide dependent (LSDn;
274 Lifton et al., 2014) scaling model and production rates based on user-defined calibration data from
275 independently dated locations. Production rates were computed using *in situ* ^{10}Be data from the
276 independently dated surface at the Promontory Point production-rate calibration site reported by
277 Lifton et al. (2015), which features well-preserved and continuously exposed surfaces following
278 the Bonneville Flood at $18,350 \pm 300$ cal. yr BP. We chose this calibration site because of its
279 proximity in space and time to the study area, following other recent reports of Pleistocene moraine
280 chronologies in the Rocky Mountains (Licciardi and Pierce, 2018; Schweinsberg et al., 2020;
281 Laabs et al., 2020), Exposure ages calculated using other commonly used calibration (e.g.
282 CRONUS-Earth primary ^{10}Be calibration data; Borchers et al., 2016) and scaling schemes (Stone
283 et al., 2000) result in apparent age differences of 3-5%.

284 Moraine ages and associated uncertainties are reported as the arithmetic mean of individual
285 boulder exposure ages and the standard error of the mean, respectively (as in Putnam et al., 2010;
286 Quirk et al., 2020). We do not account for snow cover shielding on calculated exposure ages,
287 noting that snow shielding corrections (~3%; Marcott et al., 2019) are typically less than the total
288 uncertainty associated with production rate calibration and scaling schemes (~6%; Balco, 2020).

289 **Glacier Modeling**

290 The coupled energy/mass-balance and ice-flow models used in this study were originally
291 developed by Plummer and Phillips (2003) and have been successfully used to estimate

Formatted: Font: 12 pt

292 paleoclimate conditions for extinct glaciers in a variety of geologic settings (Quirk et al., 2020;
293 Rowan et al., 2014; Leonard et al., 2014; Harrison et al., 2014; Laabs et al., 2006). Additionally,
294 several studies have verified the model's ability to successfully predict snow accumulation (Laabs
295 et al., 2006; Leonard et al., 2014) and melt (Quirk et al., 2020), as well as small glacier extents
296 (Plummer, 2002) for modern conditions in the western U.S.

297 Our modeling approach is to match simulated glacier extents produced under prescribed
298 climate perturbations relative to modern (e.g., temperature depression and precipitation change) to
299 field evidence such as terminal and lateral moraines. In this study, we match modeled glacier
300 shapes and thicknesses to the well-defined Pinedale maximum ice extents at Cut Bank, Pine Creek
301 and South Fork Deep Creek. ~~In order to~~To test the validity of the ice flow parameters used for the
302 Cut Bank Creek glacier detailed below, we reconstructed the undated Lake Creek glacier
303 immediately to south of Cut Bank at its maximum mapped extent using the same parameters. We
304 reconstructed the Cut Bank glacier using a model spatial resolution of 180 m while we used a
305 resolution of 30 m for the Pine Creek and South Fork Deep Creek glaciers, which were modeled
306 in the same domain (herein the northern Absaroka domain). We did not include Cascade Creek as
307 a target for glacier reconstructions because mapping of the glacier's exact terminal position
308 remains unresolved.

309 The energy/mass-balance model calculates snow accumulation and ablation at every cell
310 within the model domain for the time interval of interest, typically one to several years. Annual
311 mass balance depends mostly on precipitation and temperature, which are the principal inputs to
312 the model. In this study, we use a similar approach to the one used by Leonard et al. (2017a)
313 whereby we describe the monthly spatial distribution of temperature and precipitation at every cell
314 across the model domain with linear regressions of elevation and PRISM (Parameter-elevation

315 Regression on Independent Slopes Model <http://www.prism.oregonstate.edu/>; Daly et al., 2008)
316 monthly mean climatological models. It is important to note that in our simulations we change
317 monthly temperature and precipitation distributions for the entire year while glacier mass-balance
318 is primarily sensitive to ablation season temperatures and accumulation season precipitation as
319 snowfall. Secondary climate parameters include estimates of average monthly relative humidity,
320 cloudiness, and wind speed, and are taken directly or derived from a combination of RAWS and
321 NOAA COOP Station historical weather station data. We calculated average monthly cloudiness
322 for the Cut Bank and Lake Creek Canyon domains by determining the fraction of days per month
323 with precipitation (i.e. 0.5 cloudiness = 15 days of precipitation / 30 days total). For the Pine and
324 South Fork Deep Creek domain, cloudiness was estimated using the ERA-Interim 3rd generation
325 (1979-2015) reanalysis (http://cci-reanalyzer.org/reanalysis/monthly_tseries/). Wind speed (W_s)
326 was scaled for elevation from weather station data using a given weather station's reference
327 elevation ($Elevation_{REF}$) using the equation:

$$328 \quad (1) \quad W_s = W_{SREF} + (Elevation - Elevation_{REF}) * k$$

329 where W_{SREF} is wind speed at the reference elevation and k is a wind scaling factor. Here, k is
330 taken as 0.001, resulting in an additional 1 m s^{-1} average wind speed per 1000 m elevation. Average
331 monthly cloudiness is held constant at every cell and elevation within the model domain. To
332 simulate paleo-glacier extents, we varied precipitation and temperature, the two dominant climate
333 input parameters, using multiplicative and additive variations from modern, respectively. Thus, a
334 precipitation factor change of 1 is equal to modern precipitation and a temperature of depression
335 of $0 \text{ }^\circ\text{C}$ is modern temperature.

336 The primary output from the energy/mass-balance model is a mass-balance grid for model
337 domain. The mass-balance grid is input to the ice-flow model along with a digital elevation model

338 of the drainage basins. The ice-flow model designed by Plummer and Phillips (2003) used here is
339 similar to the finite-element ice sheet model described by Fastook and Chapman (1989) and
340 follows the commonly used shallow-ice approximation. Snow and ice mass is gained in the
341 accumulation zone and flows along the ice-surface gradient via deformation and sliding into the
342 ablation zone. We run glacier simulations to steady-state where the simulated terminus stabilizes
343 at a mapped moraine position. We define steady-state condition in our model runs as when the
344 integrated surface balance errors are less than 5%, and typically $\approx 0\%$, as described by Plummer
345 and Phillips (2003). The time-dependent ice-flow model is an alternating direction-implicit, space
346 -entered, finite-difference form of the continuity equation for 2-D flow:

$$347 \quad (2) \quad \partial h / \partial t = b_n - \partial q_x / \partial x - \partial q_y / \partial y$$

348 where h = ice-surface elevation, b_n = net annual mass balance, q = ice discharge per unit width,
349 and x and y are orthogonal directions of ice flow in the horizontal plane. The ice flux between
350 neighboring cells is determined by the thickness and depth-integrated flow velocity, U , which is
351 the sum of ice flow via deformation and sliding:

$$352 \quad (3) \quad U = u_d + u_s = (1-f) H^{2/5} (\tau A)^m + f (\tau B)^n$$

353 Here A is the deformation flow coefficient, B is the sliding flow coefficient, H is ice
354 thickness, f is a velocity scaling parameter, and τ is basal shear stress. The exponents m and n are
355 taken to be 3 and 2, respectively, as described by Fastook and Chapman (1989). We tuned ice flow
356 parameters A , B , and f to match simulated glacier shapes and ice thicknesses to the observational
357 record. Ice flow parameter values that simulated observed ice thicknesses well included A values
358 for the Cut Bank and northern Absaroka domains of $8.0 \text{ E-5 a}^{-1} \text{ kPa}^{-3}$ and $1.0 \text{ E-7 a}^{-1} \text{ kPa}^{-3}$, and B
359 values of $0.0015 \text{ m a}^{-1} \text{ kPa}^{-2}$, and f values of 0 and 0.5, respectively. The ice-flow parameters used

360 in northern Absaroka domain agree well with the published range of values used in previous glacier
361 flow models (Oerlemans, 1989; Plummer and Phillips, 2003; Laabs et al., 2006; Quirk et al., 2018).

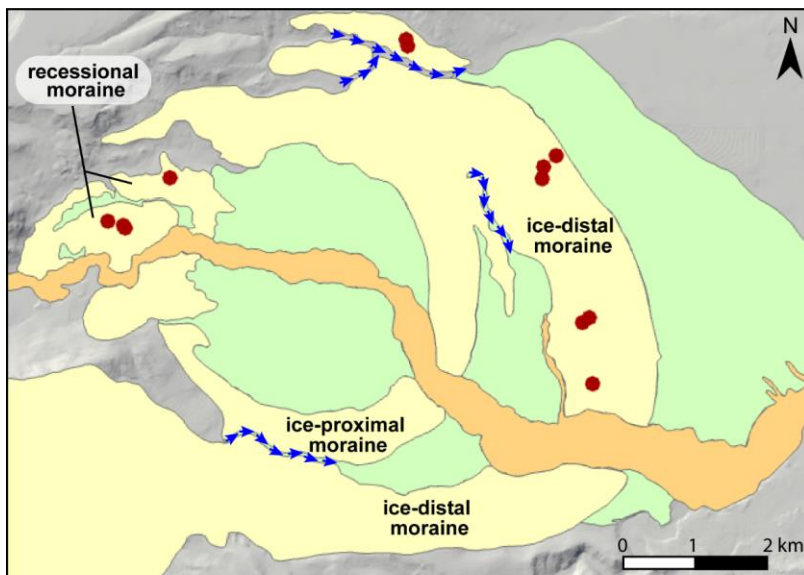
362 The Cut Bank glacier required a greater value of the deformation flow coefficient compared
363 to the steeper valley glaciers in the northern Absaroka Range. Although it is likely that the Cut
364 Bank Creek glacier was sliding at its base, we did not account for the contribution of sliding to
365 flow because it was likely far less than the contribution to flow by deformation as indicated by the
366 great ice thicknesses and low surface slopes. As described previously, we also simulated the Lake
367 Creek glacier immediately south of Cut Bank using identical ice-flow parameters to test the
368 validity of the chosen values. Through experimentation, we tuned the ice-flow parameters to
369 produce simulated steady-state glaciers that matched the mapped paleo-glacier thickness and shape
370 in both valleys and thus parameterized the effects the piedmont lobe and glacier shape had on the
371 Cut Bank glacier. (Supplemental Figure 1).

372 **RESULTS**

373 **Moraine Mapping**

374 The suite of moraines deposited at the mountain front in Cut Bank Creek valley features
375 three broad, looping plateaus with hummocky topography separated by incised meltwater channels
376 and outwash- (Figure 4). The suite includes a multi-crested terminal moraine deposited farthest
377 beyond the mountain front and a recessional moraine deposited near the mouth of Cut Bank
378 Canyon (Figure 24). The ice-distal sector of the terminal moraine has the highest internal relief
379 (up to 30 m) along the portion of the moraine south of Cut Bank Creek, with numerous closed
380 depressions, some of which are filled with shallow lakes. The distal slope of the moraine grades
381 to a broad, gently sloping outwash plain known locally as Starr School Flat, featuring low-relief
382 (<3 m) depressions and abandoned braided channels. The ice-proximal sector of the terminal

383 moraine is narrower with less internal relief (less than 15 m) and fewer closed depressions. The
384 proximal slope of this sector of the moraine appears to be partially buried by outwash where it is
385 bisected by Cut Bank Creek. The recessional moraine is best preserved north of Cut Bank Creek
386 and features low-relief hummocky topography (less than 5 m internally). In Lake Creek valley,
387 only a single, looping terminal-moraine ridge is preserved at the mountain front, forming a broad
388 area of hummocky topography with greater internal relief (up to 60 m along portions north Lake
389 Creek).



- KEY
- Pinedale till
 - Pinedale outwash
 - Alluvium
 - Ice-marginal channel
 - Sampled erratic boulder

390

391 Figure 4. Surficial geologic map of the Cut Bank Creek moraine complex detailing the Pinedale
392 ice-distal, proximal and recessional moraine extents.

393 The moraines delimit the size and shape of the piedmont lobes formed by glaciers in the
394 two valleys. ~~In Cut Bank Creek valley,~~ At Cut Bank Creek, the maximum Pinedale glacier, as
395 denoted by the ice-distal moraine, extended almost 30 km from the headwall and occupied an area
396 of ~123 km² while the piedmont lobe had a maximum diameter of 6.8 km ~~while occupying the~~
397 ~~distal sector of the moraine.~~ While occupying the ice-proximal sector, delimited by the mapped
398 recessional moraine, the Cut Bank glacier extended approximately 25 km down valley and
399 occupied an area of 86 km² while the piedmont lobe was reduced in diameter to approximately 4.4
400 km ~~and~~. The piedmont lobe likely became thinner or formed a more gradual slope near the terminus
401 as evidenced by the lower relief along the moraine. ~~The~~ As the glacier terminus subsequently
402 retreated to the recessional moraine, the piedmont glacier width was further diminished ~~upon~~
403 ~~retreat to the recessional moraine~~ to approximately 1.3 km, only slightly wider than the mouth of
404 Cut Bank Canyon. In Lake Creek valley, the piedmont lobe formed an irregular shape, likely due
405 to partial confinement of the northern side of the lobe by the right-lateral moraine in the
406 neighboring Cut Bank Creek valley. The piedmont lobe had a maximum width of about 2.5 km, a
407 total glacier length of 12 km, and occupied an area of 24 km² when the terminal moraine was
408 occupied. Upvalley of the terminal moraines in Cut Bank Creek and Lake Creek valleys, lateral
409 moraines and other glacial features mapped by Carrara (1989) were used to delimit ice thickness
410 and areal extent.

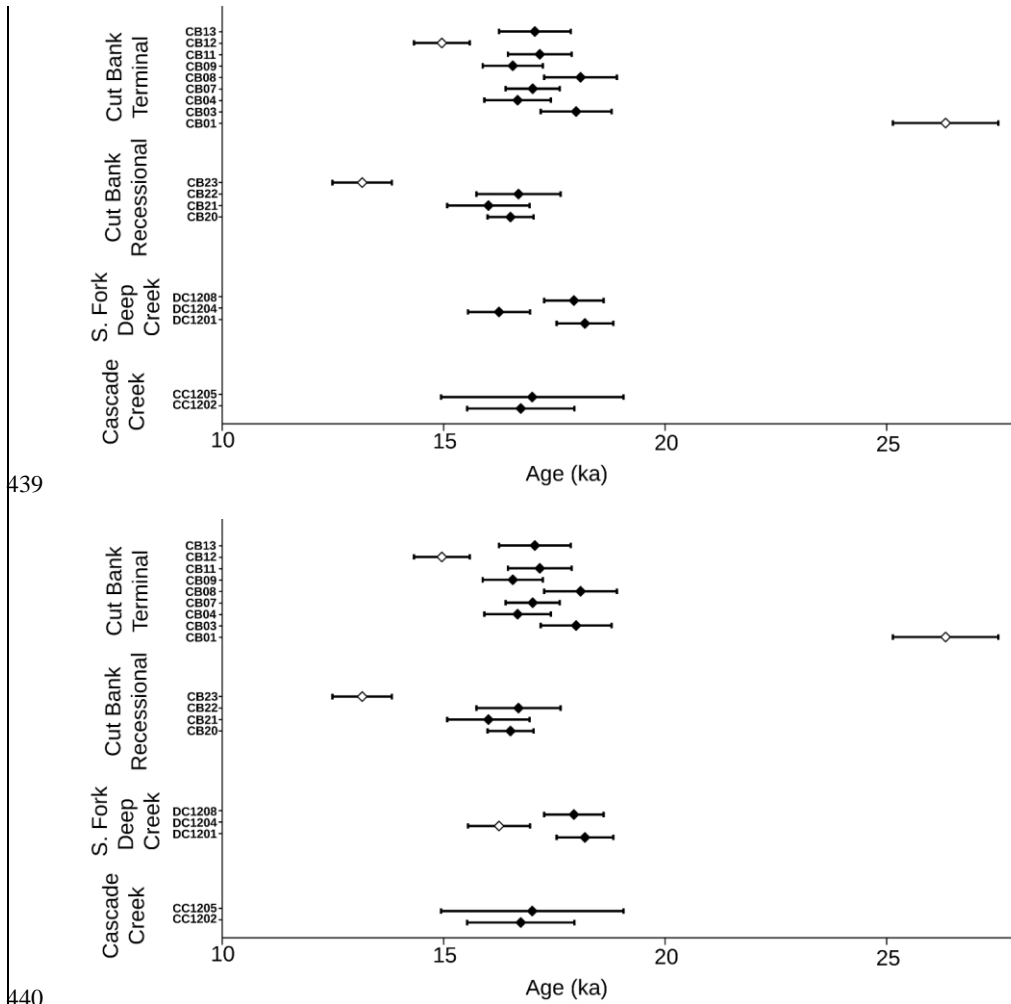
411 **Cosmogenic ¹⁰Be Exposure Ages**

412 Here we present 29 cosmogenic ¹⁰Be exposure ages collected from glaciated catchments
413 in the Lewis and northern Absaroka Ranges of Montana (Figure 2; Figure 45). In the Lewis Range,

414 nine exposure ages are from the ice-distal sector of the terminal (frontal) moraine in Cut Bank
415 Creek valley and four are from a recessional (frontal) moraine up valley. In the northern Absaroka
416 Range, two samples are from the Cascade Creek lateral moraine, three are from the South Fork
417 Deep Creek lateral moraine, and eleven are Pine Creek Canyon bedrock and erratic samples. The
418 $^{10}\text{Be}/^9\text{Be}$ ratios in procedural blanks ranged from 6.00×10^{-15} to 4.90×10^{-14} . Sample $^{10}\text{Be}/^9\text{Be}$
419 ratios ranged from 3.18×10^{-13} to 1.37×10^{-12} (Supplemental Table 1). We corrected sample
420 $^{10}\text{Be}/^9\text{Be}$ ratios by subtracting the number of ^{10}Be atoms in the corresponding blank from the
421 sample. The range of AMS measurement uncertainties (one sigma) for most samples was
422 approximately 1.5 – 3.5%. Both moraine-boulder samples from Cascade Creek have greater AMS
423 errors of 4.9% (CC12-02) and 8.3% (CC12-05).

424 We identified three outliers among moraine exposure ages, including samples CB-01,
425 CB-12 from the Cut Bank terminal and CB-23 from the Cut Bank recessional moraine (Table 1).
426 Sample CB-01 is more than 8 ka older than all other boulder exposure ages from the terminal
427 moraine and is therefore interpreted to reflect inherited ^{10}Be nuclide inventory in the surface from
428 a period of prior exposure. Sample CB-12 is younger than all but one of the exposure ages on the
429 upvalley recessional moraine, which is interpreted to represent incomplete or inconsistent
430 exposure history since the terminal moraine was deposited. Sample CB-23 has an exposure age 3
431 ka younger than the three other boulders from the moraine and is also interpreted to represent
432 incomplete or inconsistent exposure history since the recessional moraine was deposited. Although
433 we found no evidence in the field for inconsistent exposure histories among the sampled boulders,
434 these young exposure ages could be explained by several geologic processes including local burial
435 by sediment followed by exhumation, or significant boulder-surface erosion rates. The mean of
436 the remaining seven ^{10}Be exposure ages from the terminal moraine in Cut Bank Creek valley limit

437 its abandonment to 17.2 ± 0.2 ka. The abandonment age of the recessional moraine, 16.4 ± 0.2 ka,
 438 is defined by three exposure ages.



441 Figure 45. Cosmogenic ^{10}Be exposure ages with analytical uncertainties for samples collected
 442 from moraines at Cascade Creek and South Fork Deep Creek in the Absaroka Range and moraines

443 *at Cut Bank in the Lewis Range. Samples that have been identified as outliers are denoted by open*
444 *symbols.*

445 Abandonment ages for the two moraines in the northern Absaroka Range at Cascade
446 Canyon and South Fork Deep Creek are limited by the means of two ~~and three~~ boulder exposure
447 ages each at 16.9 ± 0.1 ka and ~~17.5~~18.1 ± 0.6 1 ka, respectively, although we reiterate that the
448 exposure ages of the lateral moraine at Cascade Canyon are considered preliminary because of the
449 greater-than-expected AMS measurement errors.

450 The set of bedrock exposure ages from the ice-recessional path in Pine Creek valley
451 includes one (PC11-03, 34.0 ± 2.8 ka) that exceeds the exposure age of the lateral moraine
452 downvalley (18.2 ± 0.5 ka, Licciardi and Pierce, 2008) and two (PC11-04 and PC11-10, 18.1 ± 2.1
453 and 18.3 ± 0.8 ka, respectively) that overlap with it. These surfaces are interpreted to reflect
454 inherited ^{10}Be from a period of prior exposure, which suggests that glacial scouring during the last
455 glaciation at these sample sites was insufficient to remove the ^{10}Be inherited from pre-glacial
456 exposure of the valley floor. Two samples, PC11-07 and PC11-12, yield exposure ages younger
457 than surfaces sampled at upvalley positions and are interpreted to reflect incomplete exposure due
458 to burial by sediment. Sample PC11-07 is from an erratic boulder atop a bedrock surface with
459 exposure ages 3 kyr older, suggesting that the boulder, originally interpreted to be an erratic
460 deposited by glacier ice during recession, has been reworked by fluvial and mass-movement
461 processes. The remaining six exposure ages range from 16.0 ± 0.6 ka at the farthest downvalley
462 site (PC11-11) to 13.7 ± 0.3 ka at the farthest up valley site (PC11-01) in the cirque occupied by
463 Pine Creek Lake. When combined with the mean exposure age of the latero-terminal moraine of
464 18.2 ± 0.5 ka, these exposure ages record the pace and timing of ice retreat over a period of ~4 kyr.

Table 1. Cosmogenic ¹⁰Be sample information and exposure ages

Sample ID	Latitude	Longitude	Elevation (m)	Thickness (cm)	Density (g cm ⁻²)	Shielding Factor	Erosion rate (cm yr ⁻¹)	[Be-10] (atmos g ⁻¹)	+/-	Exposure Age (ka)	Analytical Error (ka)	External Error (ka)
<i>Cut Bank Terminal Moraine</i>												
<u>CB-01</u>	<u>48.5936</u>	<u>-113.1555</u>	<u>1444</u>	<u>1</u>	<u>2.65</u>	<u>1</u>	<u>0</u>	<u>3.96E+05</u>	<u>1.78E+04</u>	<u>26.3</u>	<u>1.2</u>	<u>1.6</u>
CB-03	48.6009	-113.1577	1452	3	2.65	1	0	2.64E+05	1.17E+04	18.0	0.8	1.1
CB-04	48.6016	-113.1565	1450	3.8	2.65	1	0	2.42E+05	1.08E+04	16.7	0.8	1.0
CB-07	48.6260	-113.1673	1474	4.3	2.65	1	0	2.51E+05	8.93E+03	17.0	0.6	0.9
CB-08	48.6257	-113.1670	1472	3	2.65	1	0	2.70E+05	1.21E+04	18.1	0.8	1.1
CB-09	48.6210	-113.1633	1465	3	2.65	1	0	2.45E+05	1.00E+04	16.6	0.7	0.9
CB-11	48.6196	-113.1656	1469	3	2.65	1	0	2.55E+05	1.07E+04	17.2	0.7	1.0
<u>CB-12</u>	<u>48.6345</u>	<u>-113.1913</u>	<u>1523</u>	<u>3</u>	<u>2.65</u>	<u>1</u>	<u>0</u>	<u>2.31E+05</u>	<u>9.61E+03</u>	<u>15.0</u>	<u>0.6</u>	<u>0.8</u>
CB-13	48.6338	-113.1910	1518	2.8	2.65	1	0	2.64E+05	1.25E+04	17.1	0.8	1.0
Landform Age (ka)										17.2		
Standard Error (ka)										0.2		
<i>Cut Bank Recessional Moraine</i>												
CB-20	48.6170	-113.2336	1539	4	2.65	1	0	2.57E+05	8.07E+03	16.5	0.5	0.8
CB-21	48.6115	-113.2447	1544	4	2.65	1	0	2.50E+05	1.44E+04	16.0	0.9	1.1
CB-22	48.6111	-113.2418	1534	2	2.65	1	0	2.63E+05	1.49E+04	16.7	1.0	1.1
<u>CB-23</u>	<u>48.6108</u>	<u>-113.2414</u>	<u>1532</u>	<u>5</u>	<u>2.65</u>	<u>1</u>	<u>0</u>	<u>2.01E+05</u>	<u>1.02E+04</u>	<u>13.2</u>	<u>0.7</u>	<u>0.8</u>
Landform Age (ka)										16.4		
Standard Error (ka)										0.2		
<i>Cascade Creek</i>												
CC12-02	45.4688	-110.5449	1934	4	2.65	0.995	0	3.31E+05	2.39E+04	16.7	1.2	1.4
CC12-05	45.4666	-110.5428	1968	4	2.65	0.995	0	3.45E+05	4.17E+04	17.0	2.1	2.2
Landform Age (ka)										16.9		
Standard Error (ka)										0.1		
<i>S. Fork Deep Creek Lateral Moraine</i>												
DC12-01	45.5145	-110.5039	2093	4	2.65	0.989	0	4.05E+05	1.41E+04	18.2	0.6	0.9
DC12-04	45.5229	-110.5120	1927	4	2.65	0.993	0	3.19E+05	1.37E+04	16.3	0.7	0.9
DC12-08	45.5264	-110.5192	1815	3	2.65	0.994	0	3.28E+05	1.22E+04	17.9	0.7	1.0
Landform Age (ka)										17.5		
Standard Error (ka)										0.6		
<i>Pine Creek Bedrock and Erratic</i>												
PC11-01	45.4840	-110.4626	2761	2	2.65	0.975	0	4.84E+05	1.17E+04	13.7	0.3	0.6
<u>PC11-03</u>	<u>45.4859</u>	<u>-110.4668</u>	<u>2774</u>	<u>3</u>	<u>2.65</u>	<u>0.314</u>	<u>0</u>	<u>4.08E+05</u>	<u>3.38E+04</u>	<u>34.0</u>	<u>2.8</u>	<u>3.1</u>
<u>PC11-04</u>	<u>45.4862</u>	<u>-110.4664</u>	<u>2768</u>	<u>2</u>	<u>2.65</u>	<u>0.978</u>	<u>0</u>	<u>6.55E+05</u>	<u>7.56E+04</u>	<u>18.1</u>	<u>2.1</u>	<u>2.2</u>
PC11-05	45.4885	-110.4667	2752	2	2.65	0.955	0	5.09E+05	2.59E+04	14.7	0.8	0.9
PC11-06	45.4885	-110.4670	2757	3	2.65	0.959	0	5.18E+05	1.74E+04	15.0	0.5	0.8
<u>PC11-07</u>	<u>45.4886</u>	<u>-110.4668</u>	<u>2765</u>	<u>2.5</u>	<u>2.65</u>	<u>0.956</u>	<u>0</u>	<u>4.21E+05</u>	<u>1.47E+04</u>	<u>11.8</u>	<u>0.4</u>	<u>0.6</u>
PC11-08	45.4919	-110.4772	2509	3	2.65	0.918	0	4.03E+05	1.40E+04	14.5	0.5	0.7
PC11-09	45.4919	-110.4773	2508	3	2.65	0.918	0	4.23E+05	2.25E+04	15.2	0.8	1.0
<u>PC11-10</u>	<u>45.4912</u>	<u>-110.4873</u>	<u>2262</u>	<u>2.3</u>	<u>2.65</u>	<u>0.947</u>	<u>0</u>	<u>4.48E+05</u>	<u>2.02E+04</u>	<u>18.3</u>	<u>0.8</u>	<u>1.1</u>
PC11-11	45.4914	-110.4870	2276	3	2.65	0.940	0	3.88E+05	1.33E+04	16.0	0.6	0.8
<u>PC11-12</u>	<u>45.4898</u>	<u>-110.4939</u>	<u>2110</u>	<u>3</u>	<u>2.65</u>	<u>0.952</u>	<u>0</u>	<u>2.95E+05</u>	<u>1.03E+04</u>	<u>13.7</u>	<u>0.5</u>	<u>0.7</u>

Underlined indicates outlier samples

Table 1. Cosmogenic ¹⁰Be sample information and exposure ages

Sample ID	Latitude	Longitude	Elevation (m)	Thickness (cm)	Density (g cm ⁻²)	Shielding Factor	Erosion rate (cm yr ⁻¹)	[Be-10] (atmos g ⁻¹)	+/-	Exposure Age (ka)	Analytical Error (ka)	External Error (ka)
<i>Cut Bank Terminal Moraine</i>												
<u>CB-01</u>	<u>48.5936</u>	<u>-113.1555</u>	<u>1444</u>	<u>1</u>	<u>2.65</u>	<u>1</u>	<u>0</u>	<u>3.96E+05</u>	<u>1.78E+04</u>	<u>26.3</u>	<u>1.2</u>	<u>1.6</u>
CB-03	48.6009	-113.1577	1452	3	2.65	1	0	2.64E+05	1.17E+04	18.0	0.8	1.1
CB-04	48.6016	-113.1565	1450	3.8	2.65	1	0	2.42E+05	1.08E+04	16.7	0.8	1.0
CB-07	48.6260	-113.1673	1474	4.3	2.65	1	0	2.51E+05	8.93E+03	17.0	0.6	0.9
CB-08	48.6257	-113.1670	1472	3	2.65	1	0	2.70E+05	1.21E+04	18.1	0.8	1.1
CB-09	48.6210	-113.1633	1465	3	2.65	1	0	2.45E+05	1.00E+04	16.6	0.7	0.9
CB-11	48.6196	-113.1656	1469	3	2.65	1	0	2.55E+05	1.07E+04	17.2	0.7	1.0
<u>CB-12</u>	<u>48.6345</u>	<u>-113.1913</u>	<u>1523</u>	<u>3</u>	<u>2.65</u>	<u>1</u>	<u>0</u>	<u>2.31E+05</u>	<u>9.61E+03</u>	<u>15.0</u>	<u>0.6</u>	<u>0.8</u>
CB-13	48.6338	-113.1910	1518	2.8	2.65	1	0	2.64E+05	1.25E+04	17.1	0.8	1.0
										Landform Age (ka)	17.2	
										Standard Error (ka)	0.2	
<i>Cut Bank Recessional Moraine</i>												
CB-20	48.6170	-113.2336	1539	4	2.65	1	0	2.57E+05	8.07E+03	16.5	0.5	0.8
CB-21	48.6115	-113.2447	1544	4	2.65	1	0	2.50E+05	1.44E+04	16.0	0.9	1.1
CB-22	48.6111	-113.2418	1534	2	2.65	1	0	2.63E+05	1.49E+04	16.7	1.0	1.1
<u>CB-23</u>	<u>48.6108</u>	<u>-113.2414</u>	<u>1532</u>	<u>5</u>	<u>2.65</u>	<u>1</u>	<u>0</u>	<u>2.01E+05</u>	<u>1.02E+04</u>	<u>13.2</u>	<u>0.7</u>	<u>0.8</u>
										Landform Age (ka)	16.4	
										Standard Error (ka)	0.2	
<i>Cascade Creek</i>												
CC12-02	45.4688	-110.5449	1934	4	2.65	0.995	0	3.31E+05	2.39E+04	16.7	1.2	1.4
CC12-05	45.4666	-110.5428	1968	4	2.65	0.995	0	3.45E+05	4.17E+04	17.0	2.1	2.2
										Landform Age (ka)	16.9	
										Standard Error (ka)	0.1	
<i>S. Fork Deep Creek Lateral Moraine</i>												
DC12-01	45.5145	-110.5039	2093	4	2.65	0.989	0	4.05E+05	1.41E+04	18.2	0.6	0.9
<u>DC12-04</u>	<u>45.5229</u>	<u>-110.5120</u>	<u>1927</u>	<u>4</u>	<u>2.65</u>	<u>0.993</u>	<u>0</u>	<u>3.19E+05</u>	<u>1.37E+04</u>	<u>16.3</u>	<u>0.7</u>	<u>0.9</u>
DC12-08	45.5264	-110.5192	1815	3	2.65	0.994	0	3.28E+05	1.22E+04	17.9	0.7	1.0
										Landform Age (ka)	18.1	
										Standard Error (ka)	0.1	
<i>Pine Creek Bedrock and Erratic</i>												
PC11-01	45.4840	-110.4626	2761	2	2.65	0.975	0	4.84E+05	1.17E+04	13.7	0.3	0.6
<u>PC11-03</u>	<u>45.4859</u>	<u>-110.4668</u>	<u>2774</u>	<u>3</u>	<u>2.65</u>	<u>0.314</u>	<u>0</u>	<u>4.08E+05</u>	<u>3.38E+04</u>	<u>34.0</u>	<u>2.8</u>	<u>3.1</u>
<u>PC11-04</u>	<u>45.4862</u>	<u>-110.4664</u>	<u>2768</u>	<u>2</u>	<u>2.65</u>	<u>0.978</u>	<u>0</u>	<u>6.55E+05</u>	<u>7.56E+04</u>	<u>18.1</u>	<u>2.1</u>	<u>2.2</u>
PC11-05	45.4885	-110.4667	2752	2	2.65	0.955	0	5.09E+05	2.59E+04	14.7	0.8	0.9
PC11-06	45.4885	-110.4670	2757	3	2.65	0.959	0	5.18E+05	1.74E+04	15.0	0.5	0.8
<u>PC11-07</u>	<u>45.4886</u>	<u>-110.4668</u>	<u>2765</u>	<u>2.5</u>	<u>2.65</u>	<u>0.956</u>	<u>0</u>	<u>4.21E+05</u>	<u>1.47E+04</u>	<u>11.8</u>	<u>0.4</u>	<u>0.6</u>
PC11-08	45.4919	-110.4772	2509	3	2.65	0.918	0	4.03E+05	1.40E+04	14.5	0.5	0.7
PC11-09	45.4919	-110.4773	2508	3	2.65	0.918	0	4.23E+05	2.25E+04	15.2	0.8	1.0
<u>PC11-10</u>	<u>45.4912</u>	<u>-110.4873</u>	<u>2262</u>	<u>2.3</u>	<u>2.65</u>	<u>0.947</u>	<u>0</u>	<u>4.48E+05</u>	<u>2.02E+04</u>	<u>18.3</u>	<u>0.8</u>	<u>1.1</u>
PC11-11	45.4914	-110.4870	2276	3	2.65	0.940	0	3.88E+05	1.33E+04	16.0	0.6	0.8
<u>PC11-12</u>	<u>45.4898</u>	<u>-110.4939</u>	<u>2110</u>	<u>3</u>	<u>2.65</u>	<u>0.952</u>	<u>0</u>	<u>2.95E+05</u>	<u>1.03E+04</u>	<u>13.7</u>	<u>0.5</u>	<u>0.7</u>

Underlined indicates outlier samples

466

467 **Glacier Climate Reconstructions**

468 Model simulations were completed for the Cut Bank and northern Absaroka model
469 domains including four simulations matching the: Cut Bank terminal moraine (CB_T), Cut Bank
470 recessional moraine (CB_R), and Pine Creek and South Fork Deep Creek lateral sectors of terminal
471 moraines (NA_T; Figure 56). For simplicity, each of the sets of four simulations pin precipitation

472 change (P_x) to multiplicative factors of 0.5, 1.0, 2.0, and 3.0 times modern precipitation, while
473 temperature depressions (T_d) were independently varied in each experiment to match mapped ice
474 extents. In each of the 12 experiments, calculated ice extents and thicknesses matched well with
475 field evidence. The twelve experiments define 3 curves (Figure 67), in T_d - P_x space, representing
476 paleoclimate estimates for ice matching CB_T ($R^2 = 0.98$), CB_R ($R^2 = 0.99$) NA_T ($R^2 = 0.99$) with
477 equations:

478 (4) $CB_T \quad P_x = 24.084e^{0.3589T_d}$

479 (5) $CB_R \quad P_x = 6.3721e^{0.2417T_d}$

480 (6) $NA_T \quad P_x = 16.877e^{0.3379T_d}$

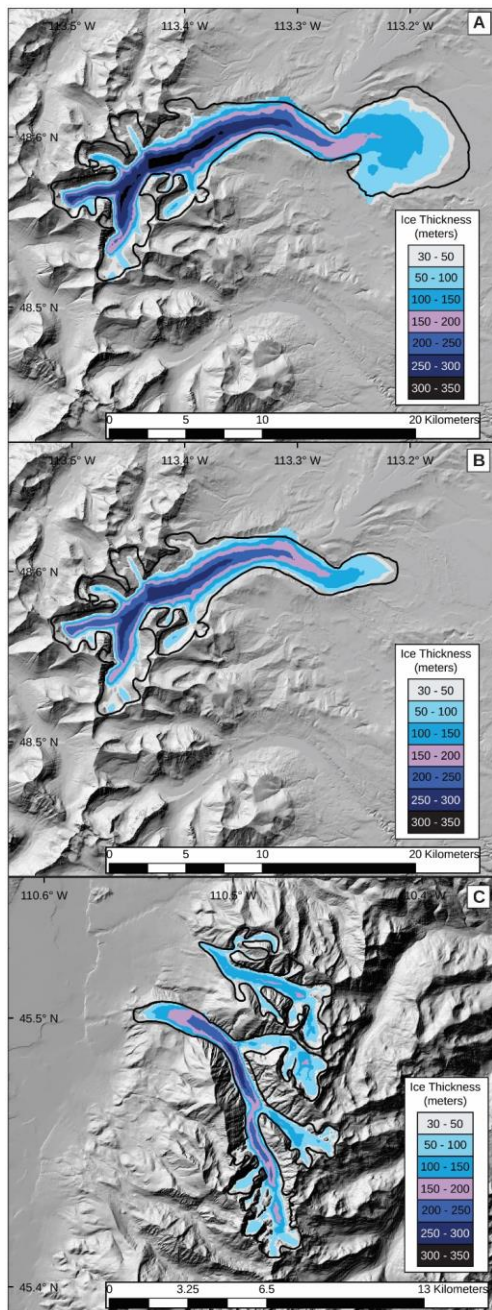


Figure 56. Ice thickness maps generated

482 from coupled energy-mass balance and ice-flow modeling for A) Cut Bank terminal B) Cut Bank
483 recessional and C) Pine Creek and South Fork Deep Creek in the Absaroka Range. Modeled ice-
484 extents were matched to field evidence (black outlines) by varying precipitation (P_x) and
485 temperature (T_d) by multiplicative and additive changes, respectively. For each simulation, we
486 found a series of P_x - T_d combinations that produced modeled ice extents that satisfactorily matched
487 field evidence. Ice extents shown here use 100% modern precipitation and temperature depressions
488 of -9.2, -8.0, and -8.5 for the Cut Bank terminal (A), Cut Bank recessional (B), and Absaroka
489 Range model domains, respectively.

490 As previously mentioned, ~~in order~~ to match the modeled glacier shape to field evidence at Cut
491 Bank, we found it necessary to effectively set the contribution of ice velocity due to sliding to zero.
492 ~~In order to~~ To test how realistic these model conditions were for reconstructing other glaciers, we
493 reconstructed the Pinedale glacier that occupied Lake Creek Canyon, the drainage immediately to
494 the south of Cut Bank. We matched the modeled glacier to the mapped Pinedale maximum in Lake
495 Creek Canyon with T_d - P_x combinations of -8°C & 100% and -6°C & 190% (Supplemental Figure
496 1). These T_d - P_x combinations are both approximately 1°C warmer than results for Cut Bank's
497 Pinedale maximum glacier given then same precipitation change. However, we find this
498 compelling evidence that the ice flow parameters we used to reconstruct the Cut Bank Pinedale
499 glacier are reasonable. The temperature discrepancy between the two sites could be 1) a result
500 temporal offset between the two maxima as we do not have a landform age for the Lake Creek
501 terminal moraine 2) a real climatic difference between the two catchments and/or 3) a reflection
502 of unaccounted for modeling error. With regards to the latter, we assume model uncertainties
503 ~~matching those reported in Quirk et al. (2020)~~ of $\pm 1.0^\circ\text{C}$ and 30% for temperature and

504 precipitation respectively determined by Quirk et al. (2020) through sensitivity analyses – which
505 would indicate overall agreement between the Cut Bank and Lake Creek simulations.

506 DISCUSSION

507 Cosmogenic exposure ages of moraines in a regional and global context

508 The ^{10}Be exposure ages presented here for the South Fork Deep Creek (~~17.5 ± 0.6 ka~~) and
509 ~~Cascade Creek (16.9 – 18.1 ± 0.1 ka)~~ lateral ~~moraines in~~ moraine agree well with the northern
510 ~~Absaroka Range are slightly younger than ages~~ landform age from the previously dated lateral
511 moraine in the neighboring Pine Creek valley in the northern Absaroka (^{10}Be exposure age = 18.2
512 ± 0.5 ka, with the standard error of ages recalculated from Licciardi and Pierce, 2008). The Cascade
513 Creek (16.9 ± 0.1 ka) moraine exhibits a younger age than both the South Fork Deep Creek and
514 Pine Creek moraines. However, and as previously discussed, the Cascade Creek moraine exposure
515 ages should be considered preliminary due to relatively high analytical uncertainties. Although
516 these moraines were deposited by discrete valley glaciers, their exposure ages are similar to ^{10}Be
517 exposure age of the nearby Eightmile terminal moraine (17.9 ± 0.4 ka, recalculated from Licciardi
518 and Pierce, 2008), the outermost moraine of the last glaciation deposited by the northern outlet
519 glacier of the Yellowstone Icecap, as well as to the age of the Chico moraine (17.1 ± 0.6 ka
520 recalculated from Licciardi and Pierce, 2008) the initial moraine deposited during recession of this
521 outlet glacier. These ages for the outermost and initial recessional ~~moraine~~ moraines in the northern
522 Yellowstone/northern Absaroka Range area in southwestern Montana are also very similar to those
523 we report here for the terminal (17.2 ± 0.2 ka) and initial recessional (16.4 ± 0.2 ka) moraines at
524 Cut Bank Creek in northwestern Montana. Taken together, these ages suggest that terminal
525 moraines in western Montana were occupied until ca. 18-17 ka and that glaciers were still near

526 their maximum lengths at ca. 17-16 ka in northern Yellowstone and in the Lewis Range, as
527 indicated by exposure ages of the recessional moraines.

528 Moraines in the northern Absaroka Range have exposure ages that fall within the middle
529 Pinedale interval, 18-16 ka, as identified in the greater Yellowstone region by Licciardi and Pierce
530 (2018) and after the end of the global LGM ([26.5-19.0 ka](#); Clark et al., 2009). During this time,
531 the Yellowstone glacier system thickened across the Yellowstone Plateau, coalesced with ice
532 masses in some neighboring mountains (such as the Beartooth, High Absaroka, and Gallatin
533 Ranges), and formed large outlet lobes, including the northern outlet that terminated just south of
534 the glaciated portion of the Northern Absaroka Range (Licciardi and Pierce, 2008, 2018). This
535 large glacier system persisted after the southwestern margin of the Laurentide Ice Sheet in northern
536 Montana began retreating (Dalton et al., 2020) and middle latitudes in the northern hemisphere
537 began warming (Shakun et al., 2015). Licciardi and Pierce (2018) suggest that enhanced westerly
538 airflow into the region during the middle Pinedale interval combined with orographic effects of
539 the thickened ice cap augmented precipitation in the northern Yellowstone region. The
540 strengthened westerly airflow across the region likely impacted valley glaciers in the northern
541 Absaroka Range, providing sufficient moisture for glaciers to persist at their maximum lengths
542 despite rising summer insolation at middle latitudes (Laskar et al., 2004) and atmospheric carbon
543 dioxide concentrations (Luthi et al., 2008). Additionally, middle latitudes in North America may
544 have remained cold for several millennia after the Laurentide Ice Sheet began retreating, as
545 suggested by the persistence of other Rocky Mountain glaciers at near-maximum extents until 17
546 ka (Laabs et al., 2020) and model-based estimates of the regional temperatures at 17 ka (Liu et al.,
547 2009; He, 2011).

548 The terminal and recessional moraines in the Lewis Range have exposure ages that also
549 fall within the middle Pinedale interval of 18-16 ka and thus may also have been responding to
550 similar climatic controls as in the Absaroka Range to the south. Alternatively, the post-LGM age
551 of these moraines could be related to the Lewis Range's proximity to the southwestern margin of
552 the Laurentide Ice Sheet. When the Shelby Lobe and other southwestern outlets of the Laurentide
553 Ice Sheet were at their maximum extent, general circulation modeling studies suggest that a large
554 area of high atmospheric pressure developed across the western dome of ice sheet resulting in
555 anticyclonic, easterly airflow along the southern margins (Thompson et al., 1993; Bartlein et al.,
556 1998). This circulation pattern likely resulted in cold and dry climate in the Lewis Range while
557 the southwestern outlets occupied their terminal moraines. Recent reconstructions of this sector of
558 the Laurentide Ice Sheet suggest that the Shelby Lobe retreated to the northeast by ca. 17 ka
559 (Dalton et al., 2020), which may have been accompanied by a weakening of easterly, anticyclonic
560 circulation at the latitude of the Lewis Range and strengthening westerly airflow that delivered
561 moisture-laden air and enhanced precipitation in the mountains. Enhanced precipitation may have
562 resulted in glacier advance to their maximum lengths after the Laurentide Ice Sheet began to
563 retreat. This effect has been suggested by previous studies, including earlier interpretations of the
564 moraine chronologies in northern Yellowstone region (Licciardi et al., 2001) and age limits on
565 moraines elsewhere in northern interior mountains (Licciardi et al., 2004; Thackray et al., 2004).
566 Licciardi and Pierce (2018) note that the range of terminal-moraine exposure ages in the
567 Yellowstone region includes some that overlap with the early Pinedale interval of 22-18 ka, which
568 includes the latter part of the global Last Glacial Maximum when some southwestern outlets of
569 the Laurentide Ice Sheet were at their maximum size. While the effect of the southwestern
570 Laurentide on regional airflow may not have impacted the Yellowstone region, it may have

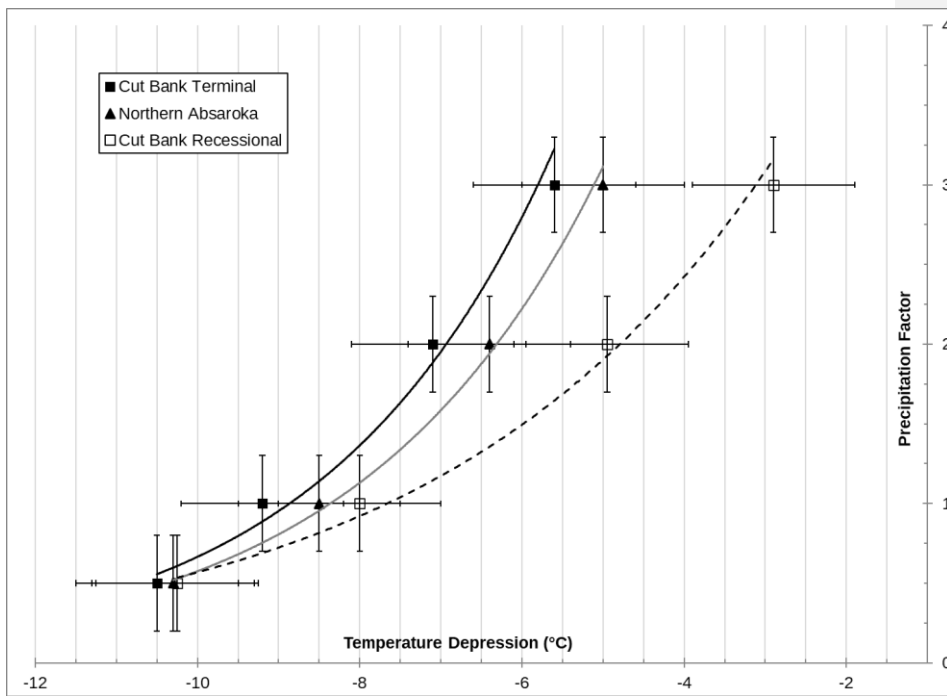
571 impacted the Lewis Range as indicated by the exposure ages of the terminal and recessional
572 moraines in Cut Bank valley. Additional age limits on moraines in the Lewis Range, other
573 mountains in northwestern Montana, and the Shelby Lobe will aid in understanding the relative
574 timing of mountain and continental glaciation.

575 Considering the glacial chronologies presented here in a larger spatial context, the exposure
576 ages of terminal and recessional moraines show some consistency with mountain glacier moraines
577 from elsewhere in the western United States. Elsewhere in the Rocky Mountains, moraines with
578 age limits of ca. 18-17 ka are found in the Sawtooth Range in Idaho (Thackray et al., 2004), the
579 Wasatch and Uinta Mountains in northern Utah, and numerous glacial valleys in the Southern
580 Rocky Mountains in Colorado (Leonard et al., 2017a; Brugger et al., 2018, 2019; Schweinsberg et
581 al., 2020). Where sequences of moraines are exposure-dated in the Rocky Mountains, the
582 outermost moraines of the last glaciation generally have ages that fall within the early Pinedale
583 interval of 22-18 ka and inner moraines (representing near-maximum glacier lengths) that fall
584 within the middle Pinedale interval (Quirk et al., 2020; Laabs et al., 2020). This pattern is observed
585 throughout the Rocky Mountains and suggests that the mountain glacier moraine chronology in
586 western Montana differs from the rest of the region, such that the outermost moraines do not
587 represent the early Pinedale interval and only represent the middle Pinedale interval- suggesting
588 similar or more extensive ice during the middle as compared to the early Pinedale. This may reflect
589 the importance of regional climatic effects on mountain glaciation, especially the strengthening of
590 westerly airflow and attendant moisture delivery, as described above.

591 **Inferred paleoclimate for the last glaciation**

592 Glacier modeling results yielded a series of P_x - T_d combinations that produced ice extents
593 that closely matched mapping-based reconstructions of the ~~for the~~ Cut Bank terminal and

594 recessional positions, and for the terminal positions in the Pine Creek and South Fork Deep Creek
595 valleys (Figure 67). Our results, particularly at Cut Bank, broadly agree with previous inferences
596 of regional Late Pleistocene climate, including pollen-based reconstructions and other applications
597 of paleoglaciology (Mumma et al., 2012; Murray and Locke, 1989; Locke, 1990; Birkel et al.,
598 2012). However, to infer changes in precipitation or temperature from our glacier modeling, one
599 of the two variables must be limited independently (i.e., from relevant paleoclimate proxy records).
600 In the following paragraphs, we consider the modeling results in the context of some existing
601 inferences of paleoclimate based on other proxy records in western Montana.



602
603 *Figure 67. Multiplicative precipitation factors and temperature depressions, both with respect to*
604 *modern, that produced modeled ice extents matching field mapped extents for 1) Cut Bank terminal*

605 *moraine 2) northern Absaroka Range Pinedale maxima at Pine Creek and South Fork Deep Creek*
606 *and 3) Cut Bank recessional moraine.*

607 Mumma et al. (2012) presented a paleoclimate record developed from Lower Red Rock
608 Lake in southwestern Montana, alongside a synthesis of other lacustrine records from the region,
609 spanning approximately from the entire LGM time interval (i.e. 26-19 ka) through the early
610 Holocene. The Lower Red Rock Lake chronology is constrained by several ¹⁴C ages from organic
611 sediments and wood, plant, and peat material as well as tephrochronology. Recalibration of
612 radiocarbon ages using ~~IntCal20~~ [IntCal13 or 20 \(Reimer et al., 2013; Reimer et al., 2020\)](#)
613 calibration data results in changes to the ages of $\leq 3\%$ and therefore does not change the
614 interpretations presented by Mumma et al. (2012). Their interpretations of the pollen and
615 sedimentological records indicate that from ca. 28-17 ka, southwestern Montana was dominated
616 by a cold and dry climate. During the subsequent interval of 17.0-10.5 ka, coinciding with regional
617 deglaciation, they suggest that temperatures increased relative to the 28-17 ka period of their record
618 but were still colder than modern and that effective moisture likely increased. Mumma et al. (2012)
619 ~~attribute~~[attributed](#) the rise in precipitation beginning at 17.0 ka to a northward migration of the jet
620 stream and increasing summer insolation. Such a shift in climate at 17 ka may be reflected in the
621 glacial chronology presented here. Increased precipitation commencing at 17 ka may have
622 augmented the mass balance of mountain glaciers resulting in ice advance to the terminal moraines.
623 A glacier response to increased regional precipitation is consistent with the assertion that increased
624 westerly airflow accompanied glacier growth in the Yellowstone region during the middle
625 Pinedale interval. Alternatively, if cold and dry climate during the interval 28-17 ka favored
626 mountain glacier maxima, then the shift to warmer and wetter climate at 17 ka may have initiated
627 ice retreat from terminal moraines.

628 Reconstructions of the valley glacier that occupied Big Timber Canyon in the Crazy
629 Mountains of western Montana by Murray and Locke (1989) provide additional limits for regional
630 climate during the last glacial culmination. Their glacier model experiments, specifically the low
631 mass-balance gradients derived from them, indicate that climate in the northeastern Crazy
632 Mountains was typical of a cold, dry continental interior, with around 75% of modern precipitation,
633 when the glacier reached its maximum size, although the specific timing of the glacier maximum
634 here is unknown. Additional work by Locke (1990, 1995) on paleoglacier reconstructions suggests
635 that last-glaciation ELAs were ~450 m lower but followed a parallel trend to those of modern
636 glacier ELAs, which he interprets to indicate similarities in temperature distributions and westerly
637 airflow across the northern Rocky Mountains of western Montana. By using the difference
638 between modern and Pleistocene ELAs to compute precipitation during the local glacial maximum
639 (for an assumed temperature depression of 10°C), Locke (1990) found that accumulation-season
640 precipitation ranged from 50 cm less than modern to 50 cm greater than modern (in units of water
641 equivalent) across mountain ranges in western Montana. However, Locke suggested that based on
642 the overall pattern of ELA change that climate in western Montana was likely drier during the
643 LGM. If precipitation changes during the last glacial culmination at 18-17 ka was 75% of modern
644 then our modeling results suggest the accompanying temperature depression in the northern
645 Absaroka Range and in the Lewis Range was around 8-10°C. The magnitude of regional climate
646 change at 18-17 ka in the Crazy Mountains is unclear, however, and may have differed between
647 the latitudes of glacial valleys in the Lewis Range (N48.6°) and that of glacial valleys in the
648 northern Absaroka (N45.5°).

649 While a unique temperature-precipitation combination for the culmination of the Pinedale
650 maximum in western Montana is difficult to infer from glacier modeling results presented here,

651 the consistent timing of the glacial culmination at 18-17 ka – after the Laurentide Ice Sheet began
652 retreating and global LGM – suggests that a regional increase in precipitation during the middle
653 Pinedale interval supported glacier maxima. This is consistent with inferred climate for the last
654 glaciation in the greater Yellowstone region described by Licciardi and Pierce (2018) and earlier
655 studies inferring that glaciers in northern mountains in the conterminous western United States
656 reached the maximum size after the Laurentide Ice Sheet began retreating (Thackray, 2008), as
657 well as the regional airflow pattern implied by the paleoglacier reconstructions of Locke (1990,
658 1995) and pollen records reported by Mumma et al. (2012). If strengthened westerly airflow at 18-
659 17 ka resulted in accumulation-season precipitation similar to modern amounts as suggested by
660 regional climate proxies and model output, then a regional temperature depression can be inferred
661 from glacier modeling results presented here. Model simulations of glaciers in the Pine Creek and
662 South Fork Deep Creek valleys suggest a temperature depression of $8.5^{\circ} \pm 1.0^{\circ}\text{C}$ in southwestern
663 Montana, whereas model simulations of the glacier in Cut Bank Creek valley suggest a temperature
664 depression of $9.2^{\circ} \pm 1.0^{\circ}\text{C}$ in northwestern Montana. This magnitude of cooling for the last glacial
665 culmination in western Montana is consistent with output of some general circulation models
666 involved in the Paleoclimate Model Intercomparison Project (PMIP3(-3)), although these results
667 represent climate at 21 ka while the Laurentide Ice Sheet was still present in western Montana- and
668 reflect average annual temperature depressions while our models likely reflect mostly changes in
669 summer temperatures. Specifically, the average annual temperature change predicted for western
670 Montana by all PMIP3 ensembles is $-12.9 \pm 4.9^{\circ}\text{C}$ (1-sigma; interpolated by Oster et al., 2015).

671 **The pace of ice retreat in the Rocky Mountains**

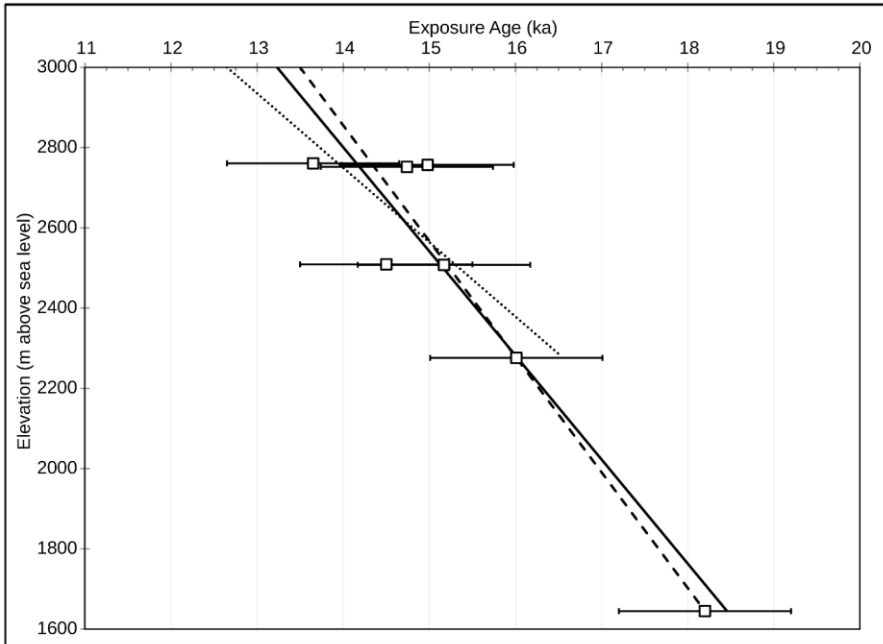
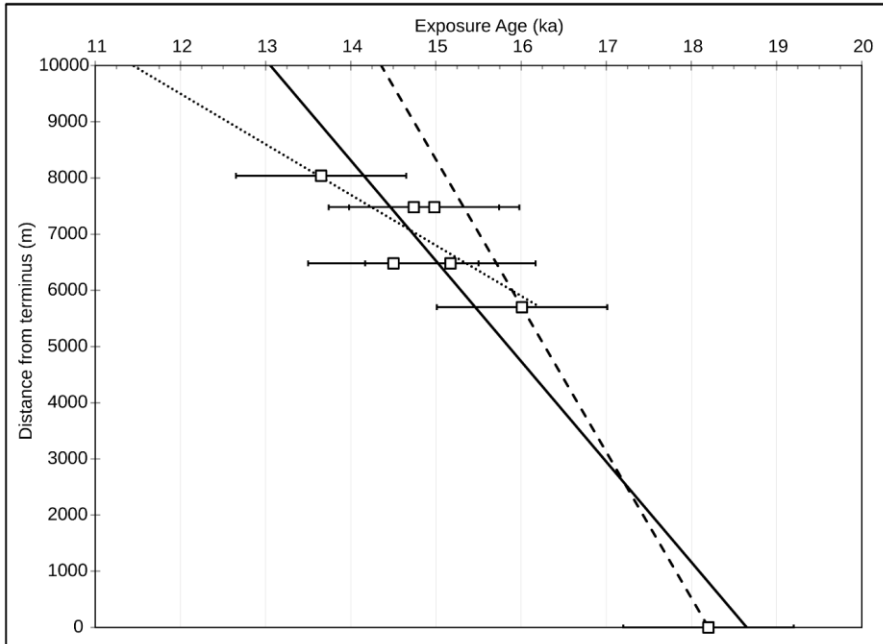
672 Ice-margin retreat rates following the abandonment of Pinedale maximum extents in the
673 northern Rockies are constrained by the cosmogenic exposure age chronology of glacially scoured

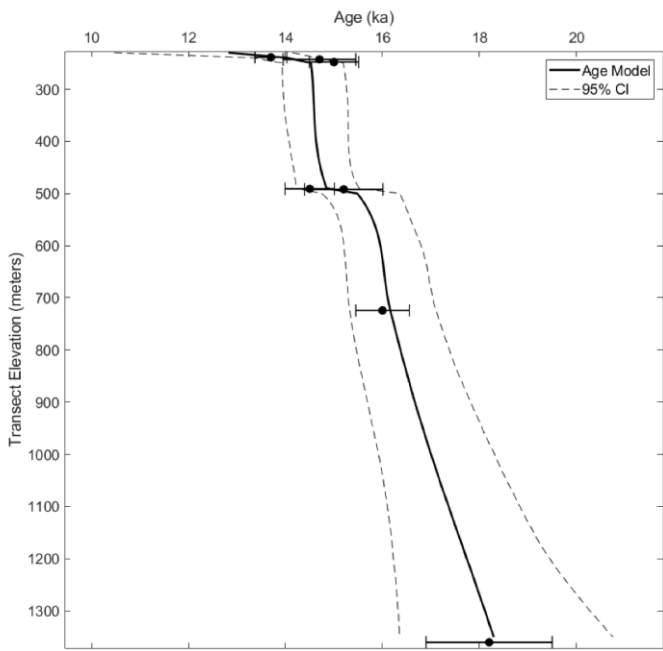
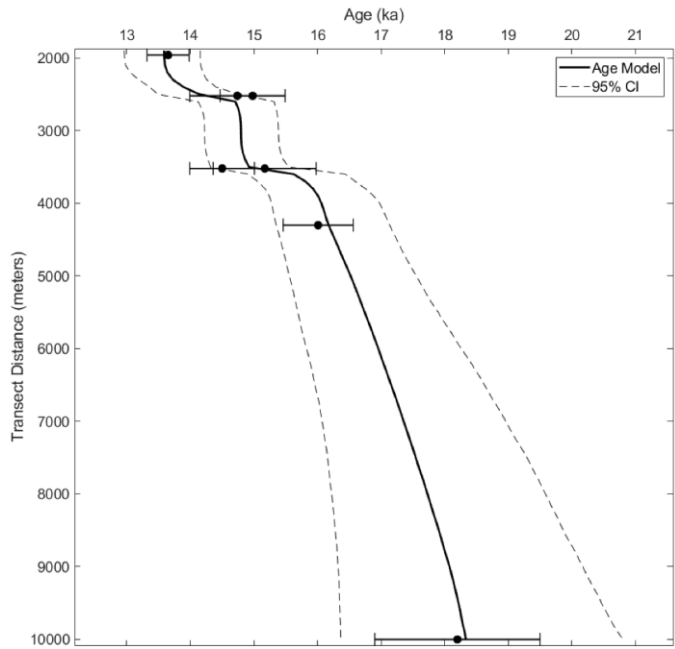
674 and striated bedrock from Pine Creek Canyon in the northern Absaroka Range (Figure 2). First,
675 we emphasize the uncertainty associated with this deglacial chronology from the exclusion of three
676 assumed old and one young outlier from the data set. Furthermore, the sample transect only
677 captures a northern tributary of the Pine Creek glacier (see sample transect in Figure 2) and thus
678 may not be representative of the larger main-valley glacier system. However, few glaciated valleys
679 in the northern Rockies have age controls sufficient to estimate retreat rates, therefore the data
680 presented here, while limited, are valuable for inferring rates of deglaciation. Keeping these
681 considerations in mind we can use the data to describe the pattern of deglaciation in the northern
682 Absaroka.

683 We ~~model the Pine Creek glacier retreat rates using linear regressions of all or select~~
684 ~~subsets of~~adapt the age ~~and sample depth~~ algorithm of Breitenbach et al. (2012) to model glacier
685 ~~age- distance~~ ~~or~~and elevation ~~data relationships~~ at Pine Creek (Figure 78). The ~~model~~algorithm
686 ~~uses a Monte Carlo scheme to estimate age- distance and elevation confidence intervals. We use~~
687 ~~10,000 age model realizations with age uncertainty perturbations equal to the exposure age~~
688 ~~analytical uncertainties. Additionally, all realizations are required to satisfy superposition and~~
689 ~~morphostratigraphic relationships. The results~~ indicate ~~median (95% confidence interval)~~
690 horizontal ice-margin retreat rates ~~ranging~~range from 1.06 km ka⁻¹ to approximately 2.64.7 km ka⁻¹
691 ¹ and vertical retreat ~~ranging~~rates from 205.221 to 288.635 m ka⁻¹. The data also suggest that the
692 main body of ice in the Pine Creek glacier had separated from the northern tributary by ca. 16 ka,
693 and by 13.7 ka, the northern tributary had undergone an 80% reduction in length and retreated over
694 1.1 km in elevation from the terminal moraine. The remaining deglacial history of the Pine Creek
695 glacier following the inferred recession around 13.7 ka is not constrained by the cosmogenic
696 chronology reported here.

697 Several studies of glaciated valleys in the western U.S. have sufficient age controls to
698 estimate retreat rates during the last glaciation along a north-south transect of the Rocky Mountains
699 including (Figure 89) the Pine Creek valley reported here, the Teton Range in Wyoming (Licciardi
700 and Pierce, 2008), the Wasatch Range and Uinta Mountains in northern Utah (Laabs et al., 2011;
701 Munroe and Laabs, 2017; Quirk et al., 2018, 2020), the Front Range (Ward et al., 2009; Duhnforth
702 et al., 2011), Sawatch Range (Briner, 2009; Young et al., 2011; Leonard et al., 2017b;
703 Schweinsberg et al., 2020; Tulenko et al., 2020), and San Juan Range (Guido et al., 2007) in
704 Colorado. Here, we consider vertical retreat rates for all sites to minimize the strong effects valley
705 slope and glacier hypsometry have on apparent rates of retreat.

706 Vertical glacier retreat rates exhibit no clear relationship with respect to latitude along a
707 north-south transect from Pine Creek in southern Montana to the San Juan Range in Colorado.
708 Retreat rates for sites in the middle of the transect (Wasatch, Uinta, Front Range) are somewhat
709 lower than rates calculated from the remaining sites and could reflect a response to increased
710 moisture at these latitudes during Heinrich Stadial 1 (e.g. Munroe and Laabs, 2013). While the
711 timing of initial abandonment of ice-distal positions is variable at sites across the Rockies,
712 ranging which range from the end of the global LGM to ca. 16 ka, the broad pattern and timing of
713 subsequent glacier retreat deglaciation after ca. 16 ka is similar across the Rocky Mountains (Figure
714 89)





716

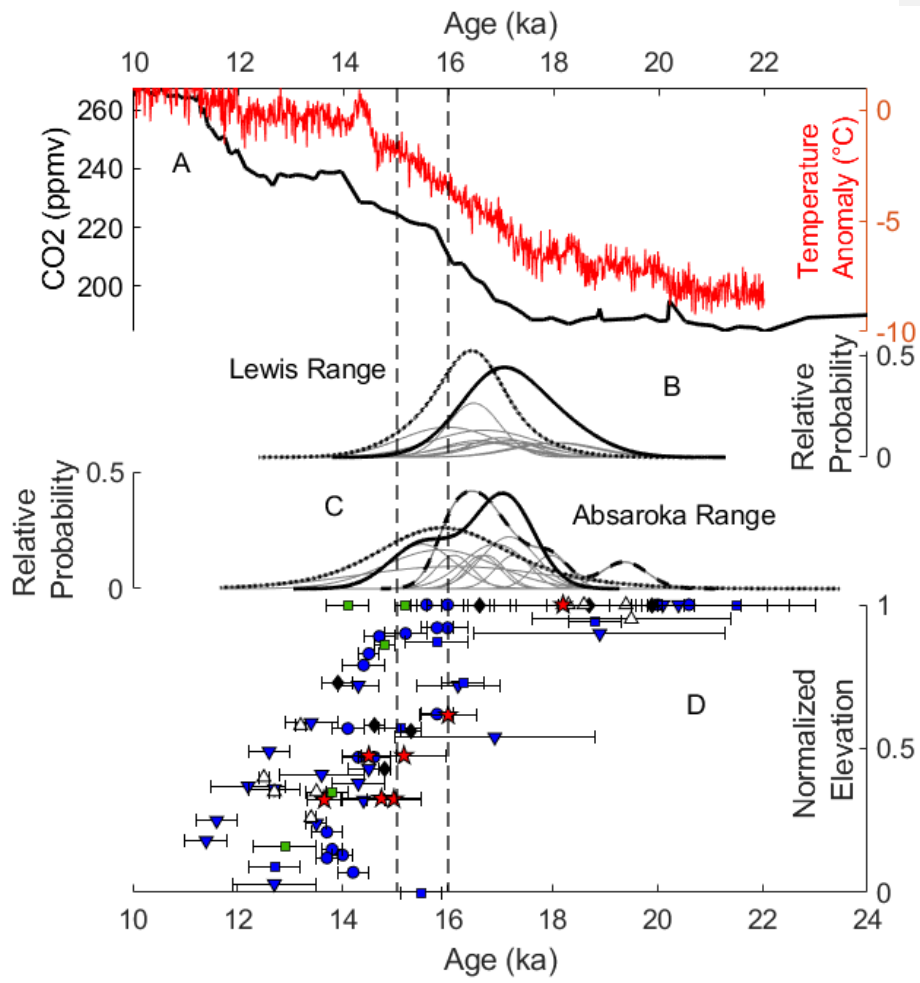
Figure 7. Time8. Age-

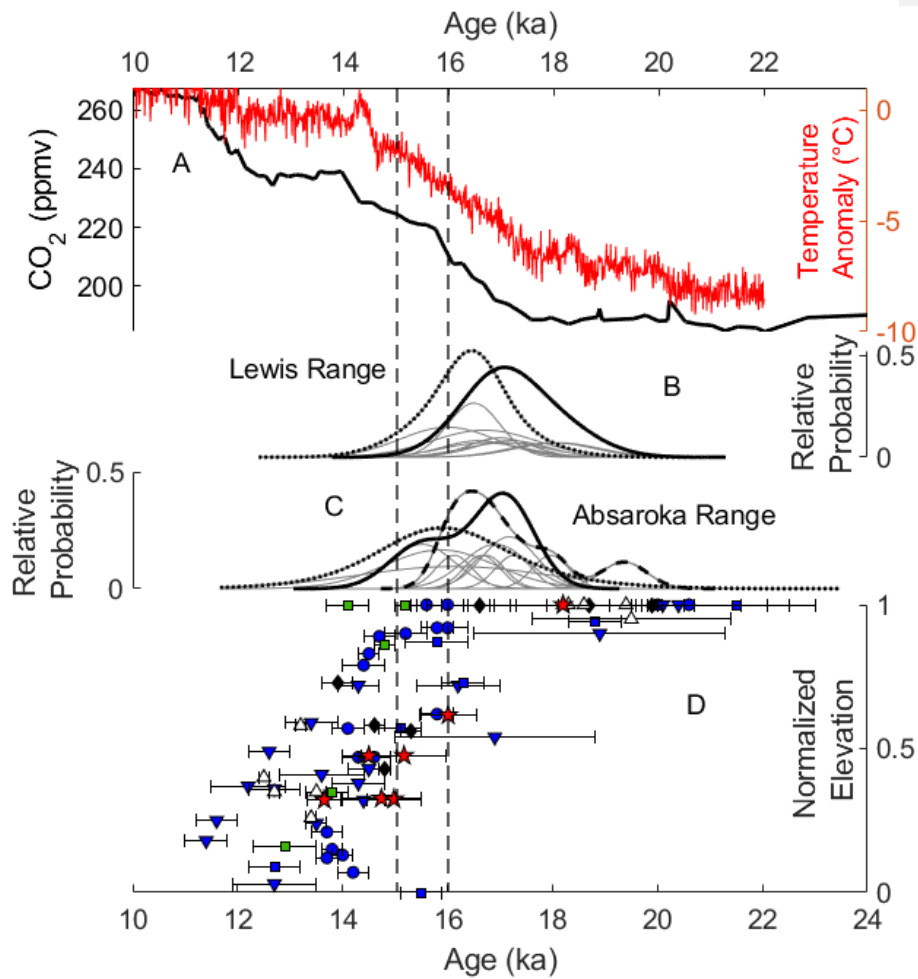
717 distance (top) and ~~time~~age-elevation (bottom) ~~diagrams illustrating~~ice retreat ~~from~~models for
718 Pine Creek. Bedrock exposure ages plotted with analytical uncertainties while the Pine Creek
719 Pinedale maximum extent (18.2 ± 1.3 ka; [Licciardi & Pierce, 2008](#)) from cosmogenic exposure
720 ages collected from striated and polished bedrock along a longitudinal transect of Pine Creek.
721 For both plots, three different retreat rates are indicated by best fit linear curves through all
722 of moraine age uncertainty is shown as the standard error. In both transects, the data (solid line),
723 lateral moraine and nearest bedrock sample (dashed line), and only bedrock ages collected in this
724 study (dotted line). All curves are extrapolatedare relative to 10 km (top) and 3000 m (bottom),
725 which are the approximate distance to and elevation of the Pine Creek headwall. Dark curves
726 represent median age models while dashed lines indicate boundaries of 95% confidence interval
727 (CI).

Formatted: Font: Italic

728 The timing of terminal moraine abandonment is variable across the Rocky Mountains and
729 span a period of around 8 ka, beginning during the LGM and continuing, such as in the Lewis and
730 Absaroka ranges, into the middle Pinedale (18-16 ka). The large range in glacier retreat from ice-
731 distal positions suggests diverse controlling mechanisms of initial deglaciation across the region.
732 However, the coherence of ice-retreat rates in the Absaroka Range with locations across the
733 Rockies from ca. 16 ka through the Lateglacial (i.e. 19–11.7 ka; [Reitner et al., 2016](#)) suggests
734 common factors driving deglaciation across the region. For example, glacier retreat in Rocky
735 Mountains after ca. 16 ka coincides with sustained increases in atmospheric CO₂ ([Petit et al., 1999](#);
736 [Monin et al., 2001](#); [Pépin et al., 2001](#)) and regional temperature changes despite some glacier
737 retreat lagging behind initial rises in CO₂ around 17 ka (Figure 89). Alternatively or in addition,
738 modeling studies have highlighted the effect North American ice-sheets, and in particular their
739 demise, have on regional climate ([Lora et al., 2016](#); [Tulenko et al., 2020](#)). Specifically, the

740 separation of the Laurentide and Cordilleran ice sheets around 15-16 ka (Dalton et al., 2020) may
741 have led to drier and warmer conditions across Western North America (Lora et al., 2016) and thus
742 may have contributed to sustained glacier retreat observed in the Rocky Mountains during this
743 time period (Figure 89). Whatever the mechanism, the data presented here highlight the dramatic
744 age-range of initial terminal moraine abandonment and regional coherence of sustained glacier
745 retreat throughout the Lateglacial.





747
 748 Figure 89. (A) Surface temperature anomalies from TRACE-21ka for Western North America
 749 ([Shakun et al., 2015](#); red) and Epica-Vostok composite CO₂ concentrations- ([Petit et al., 1999](#);
 750 [Monin et al., 2001](#); [Pépin et al., 2001](#)). (B) Camel plots of exposure age data from Cut Bank glacier
 751 in the Lewis Range: Cut Bank terminal (solid line), Cut Bank recessional (dotted line) and (C)
 752 Absaroka Range: South Fork Deep Creek (solid line), Cascade Creek (dotted line), and Pine Creek

753 (dashed line). (D) Normalized glacier elevation (*i.e.* 1 = terminus, 0 = headwall) for Pine Creek
754 glacier in the Absaroka Range (red stars), Teton Range, WY (green boxes), Wasatch Range, UT
755 (black diamonds), Uinta Mountains, UT (white triangles), Front Range, CO (blue inverted
756 triangles), Sawatch Range, CO (blue circles), and San Juan Range, CO (blue squares) based on
757 cosmogenic exposure dating. Dashed vertical lines bracket the approximate timing of the
758 separation of the Laurentide and Cordilleran ice-sheets in North America.

759 CONCLUSIONS

760 We present cosmogenic exposure ages for moraines in the Absaroka and Lewis Ranges
761 of Montana that indicate glacial stadials during the middle Pinedale interval (18-16 ka) and thus
762 after the end of the global LGM. We propose that regionally strengthened westerly airflow and
763 orographic effects associated with the thickening Yellowstone Ice Cap nourished valley glaciers
764 in the Absaroka Range with precipitation and allowed glaciers to persist at their maximum
765 lengths despite rising summer insolation at middle latitudes (Laskar et al., 2004) and rising
766 atmospheric carbon dioxide concentrations (Luthi et al., 2008). Similarly in the Lewis Range,
767 glaciers maintained their maximum extents following the retreat of the Shelby Lobe of the
768 Laurentide Ice Sheet by ca. 17 ka (Dalton et al., 2020), which we propose could have been
769 accompanied by a weakening of anticyclonic circulation and strengthening of westerly airflow
770 that effectively increased precipitation in the Lewis Range. If we assume that precipitation
771 during the middle Pinedale was similar to or slightly drier than modern, following a cold and
772 likely much drier than modern early Pinedale / LGM, our model simulations of glaciers in the
773 Absaroka Range suggest a temperature depression around $8.5\text{-}9.0^{\circ}\text{C} \pm 1.0^{\circ}\text{C}$, while model
774 simulations of the Cut Bank glacier in the Lewis Range suggest a temperature depression around
775 $9.0\text{-}10.0 \pm 1.0^{\circ}\text{C}$. Ice-retreat rates from Pine Creek Valley in the Absaroka Range likely ranged

776 ~~from 1.0 to 2.6 km/ka and vertical retreat ranging from 205 to 288 m ka⁻¹ and~~ broadly coincide
777 with other Rocky Mountain records of glacier retreat and thus may suggest regional controls.

778 **CODE & DATA AVAILABILITY**

779 Cosmogenic ¹⁰Be exposure age sample, AMS, and chemistry data are available in Table 1
780 and Supplemental Table 1. Glacier energy-mass balance and ice-flow model code available upon
781 request.

782 **COMPETING INTERESTS**

783 The authors declare that they have no conflict of interest.

784 **AUTHOR CONTRIBUTIONS**

785 Brendon Quirk, Elizabeth Huss, Benjamin Laabs, and Eric Leonard conceived the project
786 with input from Joseph Licciardi, and Mitchell Plummer. All listed co-authors completed field
787 mapping and sampling. Authors Quirk, Huss, and Laabs completed prep work for ¹⁰Be exposure
788 dating. Marc Caffee assisted with measurement of ¹⁰Be/⁹Be ratios. Brendon Quirk completed all
789 glacier modeling with significant input from the other authors. All authors contributed to data and
790 modeling interpretations. Brendon Quirk and Benjamin Laabs wrote the manuscript.

791 **ACKNOWLEDGMENTS**

792 We thank the reviewers of this manuscript in advance. We also thank Doug Steen and
793 Alec Spears for help sampling the South Fork Deep Creek and Cascade Creek moraines and with
794 preliminary glacier model results.

795 **REFERENCES**

796 Lora, J.M., Mitchell, J.L. and Tripathi, A.E., 2016. Abrupt reorganization of North Pacific and
797 western North American climate during the last deglaciation. *Geophysical Research Letters*,
798 43(22), pp.11-796.

799 Tulenko, J.P., Lofverstrom, M. and Briner, J.P., 2020. Ice sheet influence on atmospheric
800 circulation explains the patterns of Pleistocene alpine glacier records in North America. *Earth
801 and Planetary Science Letters*, 534, p.116115.

802 Alden, W.C., 1932. *Physiography and glacial geology of eastern Montana and adjacent areas* (No.
803 174). US Government Printing Office.

804 Balco, G., [2020. Glacier change and paleoclimate applications of cosmogenic-nuclide exposure
805 dating. *Annual Review of Earth and Planetary Sciences*, 48, pp.21-48.](#)

806 [Balco, G., Stone, J.O., Lifton, N.A. and Dunai, T.J., 2008. A complete and easily accessible means
807 of calculating surface exposure ages or erosion rates from ¹⁰Be and ²⁶Al measurements.
808 *Quaternary geochronology*, v. 3, p. 174-195.](#)

809 Birkel S.D., Putnam A.E., Denton G.H., Koons P.O., Fastook J.L., Putnam D.E., Maasch, K.A.
810 2012. Climate inferences from a glaciological reconstruction of the late Pleistocene Wind
811 River ice cap, Wind River Range, Wyoming. *Arctic, Antarctic, and Alpine research* 44, 265-
812 76. doi:10.1657/1938-4246-44.3.265.

813 Blackwelder, E., 1931. Pleistocene glaciation in the Sierra Nevada and Basin ranges. *Bulletin of
814 the Geological Society of America*, 42(4), pp.865-922.

815 Borchers, B., Marrero, S., Balco, G., Caffee, M., Goehring, B., Lifton, N., Nishiizumi, K., Phillips,
816 F., Schaefer, J. and Stone, J., 2016. Geological calibration of spallation production rates in the
817 CRONUS-Earth project. *Quaternary Geochronology*, v. 31, p. 188-198.

818 [Breitenbach, S.F., Rehfeld, K., Goswami, B., Baldini, J.U., Ridley, H.E., Kennett, D.J., Prufer,
819 K.M., Aquino, V.V., Asmerom, Y., Polyak, V.J. and Cheng, H., 2012. Constructing proxy
820 records from age models \(COPRA\). *Climate of the Past*, 8\(5\), pp.1765-1779.](#)

821 Briner, J.P., 2009. Moraine pebbles and boulders yield indistinguishable ¹⁰Be ages: a case study
822 from Colorado, USA. *Quaternary Geochronology*, 4(4), pp.299-305.

823 [Brugger, K.A., 2010. Climate in the southern Sawatch Range and Elk Mountains, Colorado, USA,
824 during the Last Glacial Maximum: inferences using a simple degree-day model. *Arctic,
825 Antarctic, and Alpine Research*, 42\(2\), pp.164-178.](#)

826 [Brugger, K.A.](#); Laabs, B.; Reimers, A.; Bensen, N., 2018. Late Pleistocene glaciation in the
827 Mosquito Range, Colorado, USA: Chronology and climate. *Journal of Quaternary Science*,
828 34, 187–202.

829 Brugger, K.A., Ruleman, C.A., Caffee, M.W., Mason, C.C., 2019. Climate during the Last
830 Glacial Maximum in the Northern Sawatch Range, Colorado. *Quaternary* 2, 36.
831 doi:10.3390/quat2040036.

832 Calhoun, F.H.H., 1906. The Montana lobe of the Keewatin ice sheet. (No. 50). The University of
833 Chicago Press.

834 Carrara, P.E., 1989. Late Quaternary glacial and vegetative history of the Glacier National Park
835 region, Montana (No. 1902). USGPO; For sale by the Books and Open-File Reports Section,
836 US Geological Survey.

837 Clark, P.U., Dyke, A.S., Shakun, J.D., Carlson, A.E., Clark, J., Wohlfarth, B., Mitrovica, J.X.,
838 Hostetler, S.W. and McCabe, A.M., 2009. The last glacial maximum. *Science*, v. 325, p. 710-
839 714.

840 Dalton, A.S., Margold, M., Stokes, C.R., Tarasov, L., Dyke, A.S., Adams, R.S., Allard, S., Arends,
841 H.E., Atkinson, N., Attig, J.W. and Barnett, P.J., 2020. An updated radiocarbon-based ice
842 margin chronology for the last deglaciation of the North American Ice Sheet Complex.
843 *Quaternary Science Reviews*, 234, p.106223.

Formatted: Font: Times New Roman

844 Daly, C., Halbleib, M., Smith, J.I., Gibson, W.P., Doggett, M.K., Taylor, G.H., Curtis, J. and
845 Pasteris, P.P., 2008. Physiographically sensitive mapping of climatological temperature and
846 precipitation across the conterminous United States. *International journal of climatology*, v.
847 28, p. 2031-2064.

848 Dühnforth, M. and Anderson, R.S., 2011. Reconstructing the glacial history of green lakes valley,
849 North Boulder Creek, Colorado Front Range. *Arctic, Antarctic, and Alpine Research*, 43(4),
850 pp.527-542.

851 Fastook, J.L. and Chapman, J.E., 1989. A map-plane finite-element model: three modeling
852 experiments. *Journal of Glaciology*, v. 35, p. 48-52.

853 Guido, Z.S., Ward, D.J. and Anderson, R.S., 2007. Pacing the post–Last Glacial Maximum demise
854 of the Animas Valley glacier and the San Juan Mountain ice cap, Colorado. *Geology*, 35(8),
855 pp.739-742.

856 Harrison, S., Rowan, A.V., Glasser, N.F., Knight, J., Plummer, M.A. and Mills, S.C., 2014. Little
857 Ice Age glaciers in Britain: Glacier–climate modelling in the Cairngorm mountains. *The*
858 *Holocene*, v. 24, p. 135-140.

859 Heinrich, H., 1988. Origin and consequences of cyclic ice rafting in the northeast Atlantic Ocean
860 during the past 130,000 years. *Quaternary Research*, v. 29, p. 142-152.

861 Kohl, C.P. and Nishiizumi, K., 1992. Chemical isolation of quartz for measurement of in-situ-
862 produced cosmogenic nuclides. *Geochimica et Cosmochimica Acta*, 56(9), pp.3583-3587.

863 Laabs, B.J., Marchetti, D.W., Munroe, J.S., Refsnider, K.A., Gosse, J.C., Lips, E.W., Becker, R.A.,
864 Mickelson, D.M. and Singer, B.S., 2011. Chronology of latest Pleistocene mountain glaciation
865 in the western Wasatch Mountains, Utah, U.S.A., *Quaternary Research*, v. 76, p. 272-284.

866 Laabs, B.J., Munroe, J.S., Best, L.C. and Caffee, M.W., 2013. Timing of the last glaciation and
867 subsequent deglaciation in the Ruby Mountains, Great Basin, USA. *Earth and Planetary*
868 *Science Letters*, v. 361, p. 16-25.

869 Laabs, B.J., Plummer, M.A. and Mickelson, D.M., 2006. Climate during the last glacial maximum
870 in the Wasatch and southern Uinta Mountains inferred from glacier modeling.
871 *Geomorphology*, v. 75, p. 300-317.

872 Laabs, B.J.C., and Munroe, J.S., 2016. Late Pleistocene mountain glaciation in the Lake
873 Bonneville Basin, In Oviatt, C.G., and Schroeder, J., *Lake Bonneville: A Scientific Update*,
874 Elsevier, Amsterdam, The Netherlands, p. 462-503.

875 Leonard, E.M., 1989, Climatic change in the Colorado Rocky Mountains: estimates based on modern
876 climate at late Pleistocene equilibrium lines: *Arctic and Alpine Research* 21, 245-255.

877 Leonard, E.M., Plummer, M.A., Carrara, P.E., 2014, Numerical modeling of the Snowmass
878 Creek paleoglacier, Colorado: implications for climate in the Rocky Mountains during the
879 Bull Lake glaciation (MIS 6). *Quaternary Research* 82, 533-541. doi:
880 10.1016/j.yqres.2014.03.001.

881 Leonard, E.M., Laabs, B.J., Plummer, M.A., Kroner, R.K., Brugger, K.A., Spiess, V.M.,
882 Refsnider, K.A., Xia, Y. and Caffee, M.W., 2017a. Late Pleistocene glaciation and deglaciation
883 in the Crestone Peaks area, Colorado Sangre de Cristo Mountains, USA—chronology and
884 paleoclimate. *Quaternary Science Reviews*, v. 158, p. 127-144.

885 Leonard, E.M., Laabs, B.J., Schweinsberg, A.D., Russell, C.M., Briner, J.P., Young, N.E., 2017b.
886 Glaciation in the Colorado Rocky Mountains, USA, following the last glacial maximum.
887 *Cuadernos de Investigación Geográfica* 43, 497-526. <http://doi.org/10.18172/cig.3234>

888 Licciardi, J.M. and Pierce, K.L., 2008. Cosmogenic exposure-age chronologies of Pinedale and
889 Bull Lake glaciations in greater Yellowstone and the Teton Range, USA. *Quaternary Science*
890 *Reviews*, 27(7-8), pp.814-831.

891 Licciardi, J.M. and Pierce, K.L., 2018. History and dynamics of the Greater Yellowstone Glacial
892 System during the last two glaciations. *Quaternary Science Reviews*, 200, pp.1-33.

893 Licciardi, J.M., Clark, P.U., Brook, E.J., Pierce, K.L., Kurz, M.D., Elmore, D. and Sharma, P.,
894 2001. Cosmogenic ^3He and ^{10}Be chronologies of the late Pinedale northern Yellowstone ice
895 cap, Montana, USA. *Geology*, 29(12), pp.1095-1098.

896 Lifton, N., Caffee, M., Finkel, R., Marrero, S., Nishiizumi, K., Phillips, F.M., Goehring, B., Gosse,
897 J., Stone, J., Schaefer, J. and Theriault, B., 2015. In situ cosmogenic nuclide production rate
898 calibration for the CRONUS-Earth project from Lake Bonneville, Utah, shoreline features.
899 *Quaternary Geochronology*, v. 26, p. 56-69.

900 Lifton, N., Sato, T. and Dunai, T.J., 2014. Scaling in situ cosmogenic nuclide production rates
901 using analytical approximations to atmospheric cosmic-ray fluxes. *Earth and Planetary Science*
902 *Letters*, v. 386, p. 149-160.

903 Locke, W.W., 1990. Late Pleistocene glaciers and the climate of western Montana, USA. *Arctic*
904 *and Alpine Research* 22, 1-13.

905 Locke, W.W., 1995. Modelling of icecap glaciation of the northern Rocky Mountains of
906 Montana. *Geomorphology* 14, pp.123-130.

907 [Marcott, S.A., Clark, P.U., Shakun, J.D., Brook, E.J., Davis, P.T. and Caffee, M.W., 2019. \$^{10}\text{Be}\$](#)
908 [age constraints on latest Pleistocene and Holocene cirque glaciation across the western](#)
909 [United States. *npj Climate and Atmospheric Science*, 2\(1\), pp.1-7.](#)

910 McCoy, W.D., Williams, L.D., Kay, P.A. and Diaz, H.F., 1985. Application of an energy-balance
911 model to the late Pleistocene Little Cottonwood Canyon glacier with implications regarding
912 the paleohydrology of Lake Bonneville. Problems of and prospects for predicting Great Salt
913 Lake levels: Salt Lake City, University of Utah, pp.40-53.

914 [Monnin, E., Indermühle, A., Dällenbach, A., Flückiger, J., Stauffer, B., Stocker, T.F., Raynaud,](#)
915 [D. and Barnola, J.M., 2001. Atmospheric CO2 concentrations over the last glacial termination.](#)
916 [science, 291\(5501\), pp.112-114](#)

917 Munroe, J.S. and Laabs, B.J., 2017. Combining radiocarbon and cosmogenic ages to constrain the
918 timing of the last glacial-interglacial transition in the Uinta Mountains, Utah, USA. *Geology*,
919 45(2), pp.171-174.

920 Murray, [D.R.](#) and Locke, [W.W.](#), 1989
921 [. Dynamics of the late Pleistocene Big Timber Glacier. Crazy Mountains, Montana, USA. Journal](#)
922 [of Glaciology, 35\(120\), pp.183-190.](#) Muzikar, P., Elmore, D. and Granger, D.E., 2003.
923 Accelerator mass spectrometry in geologic research. *Geological Society of America Bulletin*,
924 v. 115, p. 643-654.

925 Oerlemans, J., 1989. On the response of valley glaciers to climate change. In: Oerlemans, J. (Ed.),
926 *Glacier Fluctuations and Climate Change*. Reidel, Dordrecht, p. 353– 371.

927 Osborn, G. and Bevis, K., 2001. Glaciation in the Great Basin of the western United States.
928 *Quaternary Science Reviews*, v. 20, p. 1377-1410.

929 Oster, J.L., Ibarra, D.E., Winnick, M.J. and Maher, K., 2015. Steering of westerly storms over
930 western North America at the Last Glacial Maximum. *Nature Geoscience*, v.8, p.201.

931 [Pépin, L., Raynaud, D., Barnola, J.M. and Loutre, M.F., 2001. Hemispheric roles of climate](#)
932 [forcings during glacial-interglacial transitions as deduced from the Vostok record and LLN-](#)

933 [2D model experiments. Journal of Geophysical Research: Atmospheres, 106\(D23\), pp.31885-](#)
934 [31892.](#)

935 Petit, J.R., Jouzel, J., Raynaud, D., Barkov, N.I., Barnola, J.M., Basile, I., Bender, M., Chappellaz,
936 J., Davis, M., Delaygue, G. and Delmotte, M., 1999. Climate and atmospheric history of the
937 past 420,000 years from the Vostok ice core, Antarctica. *Nature*, v. 399, p. 429.

938 Pierce, K.L., 1973. Surficial geologic map of the Mammoth quadrangle and part of the Gardiner
939 quadrangle, Yellowstone National Park, Wyoming and Montana (No. 641).

940 Pierce, K.L., 1979. History and dynamics of glaciation in the northern Yellowstone National Park
941 area: US Geol. Survey Prof. Paper.

942 Plummer, M.A., Phillips, F.M., 2003. A 2-D numerical model of snow/ice energy balance and ice
943 flow for paleoclimatic interpretation of glacial geomorphic features. *Quaternary Science*
944 *Reviews*, v. 22, p. 1389-1406.

945 Putnam, A.E., Denton, G.H., Schaefer, J.M., Barrell, D.J., Andersen, B.G., Finkel, R.C., Schwartz,
946 R., Doughty, A.M., Kaplan, M.R. and Schlüchter, C., 2010. Glacier advance in southern
947 middle-latitudes during the Antarctic Cold Reversal. *Nature Geoscience*, 3(10), pp.700-704.

948 Quirk, B. J., Moore, J. R., Laabs, B. J., Caffee, M. W., Plummer, M. A., 2018. Termination II,
949 Last Glacial Maximum, and Lateglacial chronologies and paleoclimate from Big Cottonwood
950 Canyon, Wasatch Mountains, Utah. *Geological Society of America Bulletin* 130, 1889-1902.
951 doi:10.1030/B31967.1.

952 Quirk, B. J., Moore, J. R., Laabs, B. J., Plummer, M. A., Caffee, M. W., 2020, Latest Pleistocene
953 glacial and climate history of the Wasatch Range, Utah. *Quaternary Science Reviews* 238,
954 106313, 1-17. Doi: 10.1016/j.quascirev.2020.106313.

955 Reimer, P.J., Austin, W.E., Bard, E., Bayliss, A., Blackwell, P.G., Ramsey, C.B., Butzin, M.,
956 Cheng, H., Edwards, R.L., Friedrich, M. and Grootes, P.M., 2020. The IntCal20 Northern
957 Hemisphere radiocarbon age calibration curve (0–55 cal kBP). *Radiocarbon*, 62(4), pp.725-
958 757. Rowan, A.V., Brocklehurst, S.H., Schultz, D.M., Plummer, M.A., Anderson, L.S. and
959 Glasser, N.F., 2014. Late Quaternary glacier sensitivity to temperature and precipitation
960 distribution in the Southern Alps of New Zealand. *Journal of Geophysical Research: Earth
961 Surface*, v. 119, p. 1064-1081.

962 [Reitner, J.M., Ivy-Ochs, S., Drescher-Schneider, R., Hajdas, I. and Linner, M., 2016.](#)
963 [Reconsidering the current stratigraphy of the Alpine Lateglacial: Implications of the](#)
964 [sedimentary and morphological record of the Lienz area \(Tyrol/Austria\). *E&G Quaternary*](#)
965 [Science Journal](#), 65(2), pp.113-144.

966 Schweinsberg, A.D., Briner, J.P., Licciardi, J.M., Shroba, R.R., Leonard, E.M., 2020.
967 Cosmogenic ¹⁰Be exposure dating of Bull Lake and Pinedale glaciations and deglaciation in
968 the upper Arkansas River valley, Colorado Rocky Mountains, U.S.A. *Quaternary Research*,
969 97. <http://doi: 10.1017/qua.2020.21>,

970 Shakun, J.D., Clark, P.U., He, F., Lifton, N.A., Liu, Z. and Otto-Bliesner, B.L., 2015. Regional
971 and global forcing of glacier retreat during the last deglaciation. *Nature communications*, v. 6.

972 [Stone, J.O., 2000. Air pressure and cosmogenic isotope production. *Journal of Geophysical*](#)
973 [Research: Solid Earth](#), 105(B10), pp.23753-23759.

974 Thackray, G.D., 2008. Varied climatic and topographic influences on Late Pleistocene mountain
975 glaciation in the western United States. *Journal of Quaternary Science*, v. 23, p.671-681.

Formatted: Font: Times New Roman

Formatted: Font: Times New Roman, Not Superscript/
Subscript

Formatted: Font: Times New Roman

Formatted: Font: Times New Roman, Not Italic

Formatted: Font: Times New Roman

Formatted: Default Paragraph Font, Font: Times New
Roman

Formatted: Font: Times New Roman

976 Thackray, G.D., Lundeen, K.A. and Borgert, J.A., 2004. Latest Pleistocene alpine glacier advances
977 in the Sawtooth Mountains, Idaho, USA: reflections of midlatitude moisture transport at the
978 close of the last glaciation. *Geology*, 32(3), pp.225-228.

979 Uppala, S.M., Kållberg, P.W., Simmons, A.J., Andrae, U., Bechtold, V.D., Fiorino, M., Gibson,
980 J.K., Haseler, J., Hernandez, A., Kelly, G.A. and Li, X., 2005. The ERA-40 re-analysis.
981 *Quarterly Journal of the royal meteorological society*, v. 131, p. 2961-3012.

982 Ward, D.J., Anderson, R.S., Guido, Z.S. and Briner, J.P., 2009. Numerical modeling of
983 cosmogenic deglaciation records, Front Range and San Juan mountains, Colorado. *Journal of*
984 *Geophysical Research: Earth Surface*, 114(F1).

985 Weed, W.H., 1893. The glaciation of the Yellowstone valley north of the park (No. 104). US
986 Geological Survey.

987 Young, N.E., Briner, J.P., Leonard, E.M., Licciardi, J.M. and Lee, K., 2011. Assessing climatic
988 and nonclimatic forcing of Pinedale glaciation and deglaciation in the western United States.
989 *Geology*, v. 39, p. 171-174.

990

Formatted: Indent: Left: 0 cm, First line: 0 cm